

## Article

# Hydrogen-Free Deoxygenation of Oleic Acid and Industrial Vegetable Oil Waste on CuNiAl Catalysts for Biofuel Production

Jose Sabino <sup>1</sup>, Denisson O. Liborio <sup>1</sup>, Santiago Arias <sup>1</sup>, Juan F. Gonzalez <sup>1</sup>, Celmy M. B. M. Barbosa <sup>1</sup>, Florival R. Carvalho <sup>2</sup>, Roger Frety <sup>1</sup>, Ivoneide C. L. Barros <sup>3,\*</sup> and Jose Geraldo A. Pacheco <sup>1,\*</sup>

<sup>1</sup> Laboratory of Refining and Cleaner Technology (LabRefino/Lateclim), Institute for Petroleum and Energy Research (LITPEG), Department of Chemical Engineering, Center of Technology and Geosciences, Federal University of Pernambuco, Recife 50740-540, PE, Brazil; celmy@ufpe.br (C.M.B.M.B.)

<sup>2</sup> Fuel Laboratory, Institute for Petroleum and Energy Research (LITPEG), Department of Chemical Engineering, Center of Technology and Geosciences, Federal University of Pernambuco, Recife 50740-540, PE, Brazil

<sup>3</sup> Department of Chemistry, Federal Rural University of Pernambuco, Recife 52171-900, PE, Brazil

\* Correspondence: ivoneide.lopes@ufrpe.br (I.C.L.B.); jose.pacheco@ufpe.br (J.G.A.P.)

**Abstract:** The pyrolysis of vegetable oil waste is an alternative way to convert biomass into high-quality second-generation biofuels, with social, economic and environmental sustainability. The present work deals with the pyrolysis of oleic acid as a model compound and an industrial vegetable oil residue on CuNiAl mixed oxide catalysts, derived from layered double hydroxides. Reactions of the oils pre-adsorbed on the catalysts (catalyst:oil mass ratio of 5:1) were performed at 550 °C on a micro-pyrolysis system and the analyses of volatile products were carried out online using GC/MS. Copper addition to NiAl catalysts increased the cracking of oleic acid. Increasing copper content also decreased the formation of aromatics and coke precursors, as well as oxygenated compounds. The CuNiAl catalyst with a Cu/Ni ratio of 0.4 showed strong catalytic activity in the conversion of an industrial vegetable oil residue with a high volume of free fatty acids produced. Compared to the non-catalytic reaction, the catalyst reduced the content of oxygenates and increased the content of hydrocarbons, particularly in the gasoline range (C5–C9). The CuNiAl oxide catalyst was able to convert vegetable oil residues into hydrocarbons in the range of gasoline, kerosene and diesel, and also linear alkylbenzenes as chemical precursors for surfactant production.

**Keywords:** pyrolysis; cracking; residues; vegetable oil; biofuel



**Citation:** Sabino, J.; Liborio, D.O.; Arias, S.; Gonzalez, J.F.; Barbosa, C.M.B.M.; Carvalho, F.R.; Frety, R.; Barros, I.C.L.; Pacheco, J.G.A. Hydrogen-Free Deoxygenation of Oleic Acid and Industrial Vegetable Oil Waste on CuNiAl Catalysts for Biofuel Production. *Energies* **2023**, *16*, 6131. <https://doi.org/10.3390/en16176131>

Academic Editors: Carmen Otilia Rusănescu and Nicoleta Ungureanu

Received: 31 July 2023

Revised: 15 August 2023

Accepted: 19 August 2023

Published: 23 August 2023



**Copyright:** © 2023 by the authors. Licensee MDPI, Basel, Switzerland. This article is an open access article distributed under the terms and conditions of the Creative Commons Attribution (CC BY) license (<https://creativecommons.org/licenses/by/4.0/>).

## 1. Introduction

The growing demand from the international community to reduce fossil greenhouse gas emissions has favored the development of sustainable means of fuel production. The production of renewable biofuels from vegetable oils and biomass residues has been shown to be an attractive alternative [1]. In the first generation of biofuels, some technologies involve the use of glucose in the production of bioethanol [2] and the use of vegetable oils and animal fats in the production of biodiesel by transesterification [3–6] or esterification [7,8]. The physical and chemical properties of these biofuels, however, limit their application as a drop-in fuel [9]. Another negative point is that the raw materials used for the production of bioethanol and first-generation biodiesel compete with food production [10]. Thus, new processes are required to convert biomass residues into high-quality fuels with social and economic sustainability.

In the sustainable production of second-generation biofuels, pyrolysis has been recognized as one of the most promising routes [11]. The pyrolysis of biomass under an inert gas produces bio-oil, biochar and syngas [12]. Second-generation biofuels are produced from waste raw materials that do not compete with food [13]. Some of these are industrial

residues from the manufacture and use of vegetable oils [14–18], vegetable oil residues [19], oily biomass residues [20,21] and animal fat [22,23].

Despite the numerous advantages of using pyrolysis in the transformation of biomass residues, technological advances are still needed to obtain more deoxygenated products. Pyrolysis bio-oil contains a variety of oxygenated compounds that produce undesirable characteristics in the fuel, such as chemical instability, low heat of combustion and high corrosivity [24,25]. Methods for the deoxygenation of bio-oil are catalytic hydrodeoxygenation (HDO) and hydrocracking [26–28]. However, HDO has problems such as high hydrogen consumption and the need to operate at high pressures [29]. Given this, the direct production of a bio-oil with low oxygen content by the catalytic pyrolysis is an attractive proposition.

It is known that the use of catalysts in pyrolysis can induce the formation of desirable compounds, promoting reactions such as aromatization, dehydrogenation, deoxygenation and cracking [30–32]. Fast catalytic pyrolysis has been studied as an alternative to produce a bio-oil with lower oxygen content and hydrocarbons as products [9,33]. Therefore, the development and application of catalysts that are selective for the products of interest are of great importance, to produce fuels with the quality required by the transport sector [34–37]. Combining low cost with satisfactory catalytic performance, catalysts based on transition metal oxides (e.g., NiO, ZnO, CeO<sub>2</sub>, Fe<sub>2</sub>O<sub>3</sub>, CuO) have been studied in pyrolysis [38–43]. The presence of nickel favors the hydrogenation and hydrogenolysis ability [39,43–45]. However, nickel catalysts are subject to deactivation by carbon deposition and sintering [46]. The addition of copper helps the Ni dispersion, decreases coke formation, and increases catalytic activity [39,47]. Zheng et al. [39] used Ni–Cu supported on MCM-41 in the pyrolysis of oleic acid and concluded that the addition of copper suppressed catalytic deactivation.

Other catalysts combine the use of Al<sub>2</sub>O<sub>3</sub>, SiO<sub>2</sub> or zeolites [48–50] to modulate the acid–base characteristics and promote cracking and deoxygenation reactions [40]. Alumina (Al<sub>2</sub>O<sub>3</sub>) has been reported to be an efficient support in the decomposition of fatty acids and triglycerides, in view of the strong interaction of these compounds with its surface [45,46,51]. In addition to its use as a support, alumina can compose mixed oxides derived from layered double hydroxides (LDHs) [38]. LDHs are widely used as precursors to obtain, after calcination, thermally stable mixed oxides with high surface area [52,53]. Arias et al. [44] investigated the pyrolysis of myristic acid using NiAl mixed oxides derived from LDHs and reported a significant influence of the metallic composition on fatty acid conversion and selectivity for hydrocarbons and oxygenated compounds. Therefore, the modulation of the metallic composition in precursors of the LDH type, aiming to explore acidic properties and intermetallic synergistic effects, can maximize the catalytic activity and stability of mixed oxides, as well as the selectivity for compounds of interest.

The present study aimed to evaluate the influence of Cu on NiAl mixed oxides, derived from layered double hydroxides, on the deoxygenation of oleic acid and an industrial vegetable oil residue, by hydrogen-free pyrolysis, for second-generation biofuel production.

## 2. Materials and Methods

### 2.1. Materials

The reagents Ni(NO<sub>3</sub>)<sub>2</sub>·6H<sub>2</sub>O (Neon, Suzano, SP, Brazil, 99%), Al(NO<sub>3</sub>)<sub>3</sub>·9H<sub>2</sub>O (Dinâmica, Indaiatuba, SP, Brazil, 98.5%), Cu(NO<sub>3</sub>)<sub>2</sub>·2.5H<sub>2</sub>O (Sigma-Aldrich, Saint Louis, MO, USA, 99%), NaOH (Neon, 99%) and terephthalic acid (Sigma-Aldrich, 99%), were used, without further purification, in the synthesis of the mixed oxides precursors. Oleic acid (Dinâmica, 99%) and a vegetable oil waste from the food industry, containing triglycerides and 37% free fatty acids, were used as substrates in the pyrolysis reactions.

### 2.2. Catalyst Preparation

LDH-type precursors were prepared by the coprecipitation method with a low degree of supersaturation, as previously described [38]. Based on the formula [M(II)<sub>1-x</sub>M(III)<sub>x</sub>(OH)<sub>2</sub>]<sup>x+</sup>

$[A^{n-}]_{x/n} \cdot mH_2O$ , with molar fraction  $x = 0.7$  ( $x = Al/(Ni + Cu + Al)$ ), the metallic compounds Ni(II), Cu(II) and Al(III) were used. Terephthalate ( $C_8H_4O_4^{2-}$ ) was used as a compensation anion with an excess of 10 mol%. The precursors were prepared with different Cu/Ni ratios: 0, 0.1, 0.2 and 0.4, which are named as NiAl-LDH, 0.1CuNiAl-LDH, 0.2CuNiAl-LDH and 0.4CuNiAl-LDH, respectively. Initially, two solutions of 200 mL each were prepared: a solution containing terephthalic acid ( $0.19 \text{ mol L}^{-1}$ ) as a source of the compensation anion, together with NaOH ( $1.0 \text{ mol L}^{-1}$ ), and another solution containing the metals, whose precursors were nitrate salts. The deionized water used to prepare the solutions was previously heated to boiling to remove  $CO_2$ . The prepared solutions were added simultaneously and slowly to a solution of deionized water heated to  $50 \text{ }^\circ\text{C}$ , under vigorous agitation, keeping the pH in the range between 6.3–6.8. The resulting mixture was maintained at  $50 \text{ }^\circ\text{C}$ , under stirring, for a period of 4 h, after which the heating was turned off and the stirring was maintained for another 16 h, at room temperature. The resulting solids were filtered under vacuum and washed with deionized water heated to  $70 \text{ }^\circ\text{C}$ , until neutral pH, and dried at  $80 \text{ }^\circ\text{C}$  for 24 h. To obtain the mixed-oxide catalysts, identified as NiAl, 0.1CuNiAl, 0.2CuNiAl and 0.4CuNiAl, the precursors were calcined under static air at  $500 \text{ }^\circ\text{C}$  ( $10 \text{ }^\circ\text{C min}^{-1}$ ) for 3 h.

### 2.3. Characterization

The metal composition of the mixed-oxide catalysts was determined by an energy dispersive X-ray fluorescence (EDX) technique. The analyses were carried out in triplicate, in a Rigaku NEX DE VS spectrometer (Tokyo, Japan) with 100 s irradiation time, helium atmosphere, Na-U channel, 60 kV voltage and  $200 \text{ } \mu\text{A}$  current. The FTIR spectra were obtained with 30 scans per sample in a Bruker Tensor II spectrometer (Billerica, MA, USA), with an ATR module, in the range  $4000\text{--}850 \text{ cm}^{-1}$ . Thermogravimetric analyses (TGAs) were performed in a NETZSCH STA 449 F3 Jupiter thermal analyzer (Waldkraiburg, Germany), under synthetic air atmosphere ( $50 \text{ mL min}^{-1}$ ), using 10 mg of sample and a heating rate of  $10 \text{ }^\circ\text{C min}^{-1}$  up to  $900 \text{ }^\circ\text{C}$ .

X-ray diffraction (XRD) analyses were conducted in a Rigaku diffractometer, model SmartLab SE, with Cu-K $\alpha$  radiation (40 kV, 30 mA), step of  $0.02^\circ$  and speed of  $2^\circ \text{ min}^{-1}$ , in the range of  $3\text{--}70^\circ$  ( $2\theta$ ) for all samples. Temperature-programmed reduction (TPR) analyses were carried out in a Micrometrics Chemisorb 2070 analyzer (Ottawa, Canada). For the analysis, 20 mg of each sample was initially pre-treated under  $20 \text{ mL min}^{-1}$   $N_2$  flow at  $300 \text{ }^\circ\text{C}$  for 1 h, using a  $10 \text{ }^\circ\text{C min}^{-1}$  ramp. Catalyst reduction was performed under  $20 \text{ mL min}^{-1}$   $H_2$  (10%) flow, diluted in argon, at a rate of  $10 \text{ }^\circ\text{C min}^{-1}$  from  $25 \text{ }^\circ\text{C}$  to  $1000 \text{ }^\circ\text{C}$ .

The textural analyses of the mixed-oxide catalysts were carried out in a Micromeritics ASAP 2020 analyzer, by quantifying the adsorption and desorption of  $N_2$  to calculate the surface area and porosity using the Brunauer–Emmett–Teller (BET) and Barrett–Joyner–Halenda (BJH) models. Approximately 0.4 g of each catalyst was initially degassed under vacuum at  $300 \text{ }^\circ\text{C}$  and quantification of  $N_2$  adsorption and desorption was performed at  $-196 \text{ }^\circ\text{C}$ , in a relative pressure range ( $P/P_0$ ) from 0.02 to 0.99.

### 2.4. Fast Pyrolysis Experiments

Prior to pyrolysis, the mixed oxides were dried at  $110 \text{ }^\circ\text{C}$  for 24 h and mixed with the substrates (oleic acid or vegetable oil residue) under manual agitation. The fast pyrolysis experiments were conducted in duplicate using a Frontier Tandem Rx-3050TR  $\mu$ -reactor (Fukushima, Japan) with helium as the carrier gas. The mass ratio used between catalysts and substrates was 5:1. Initially, 200  $\mu\text{g}$  of pure substrates and 1200  $\mu\text{g}$  of the substrate/catalyst mixtures were weighed in steel cups (Eco-Cup LF-Frontier), and quartz wool was placed over each sample to prevent loss of solid. For each experiment, a cup with sample was placed in the reactor at  $550 \text{ }^\circ\text{C}$ , and kept at that temperature for 18 s; then, the pyrolysis volatile products passed through an interface at  $300 \text{ }^\circ\text{C}$ . The products were analyzed online using a Shimadzu GC/MS QP2020 (Kyoto, Japan) with a SH-Rtx-5 column

(60 m × 0.25 mm × 0.25 μm), injector temperature of 280 °C and split ratio of 1:80. The following temperature programming was used: 40 °C for 5 min and heating at a rate of 5 °C min<sup>-1</sup> up to 280 °C, which was held for 20 min. The GC/MS interface and ion source were heated at 290 °C and 280 °C, respectively, and the data acquisition was in scan mode (40–400 *m/z*). The products were identified with similarity equal to or higher than 85% by comparison with the NIST library.

### 3. Results

#### 3.1. Characterization of Precursors and Catalysts

According to the catalysts EDX elemental analysis results from Table 1, the molar ratio  $x = \text{Al}/(\text{Al} + \text{Ni} + \text{Cu})$  differed from the theoretical value (0.7), indicating a lower incorporation of Al<sup>3+</sup> in the structure of the materials. This can be explained by the high aluminum content that was initially intended to be incorporated into the material, and which is normally not achieved, as commonly reported in the literature [38,54]. Therefore, the successive washings with water to eliminate nitrates and sodium may have caused aluminum leaching. However, Cu/Ni molar ratio values were close to the theoretical ones in all mixed oxides. No significant difference was observed in the  $x$  value between the catalysts (0.55–0.59), enabling a study of the Cu/Ni ratio effect on the material properties and pyrolysis products.

**Table 1.** Metal composition (wt.%) of the NiAl and CuNiAl mixed-oxide catalysts.

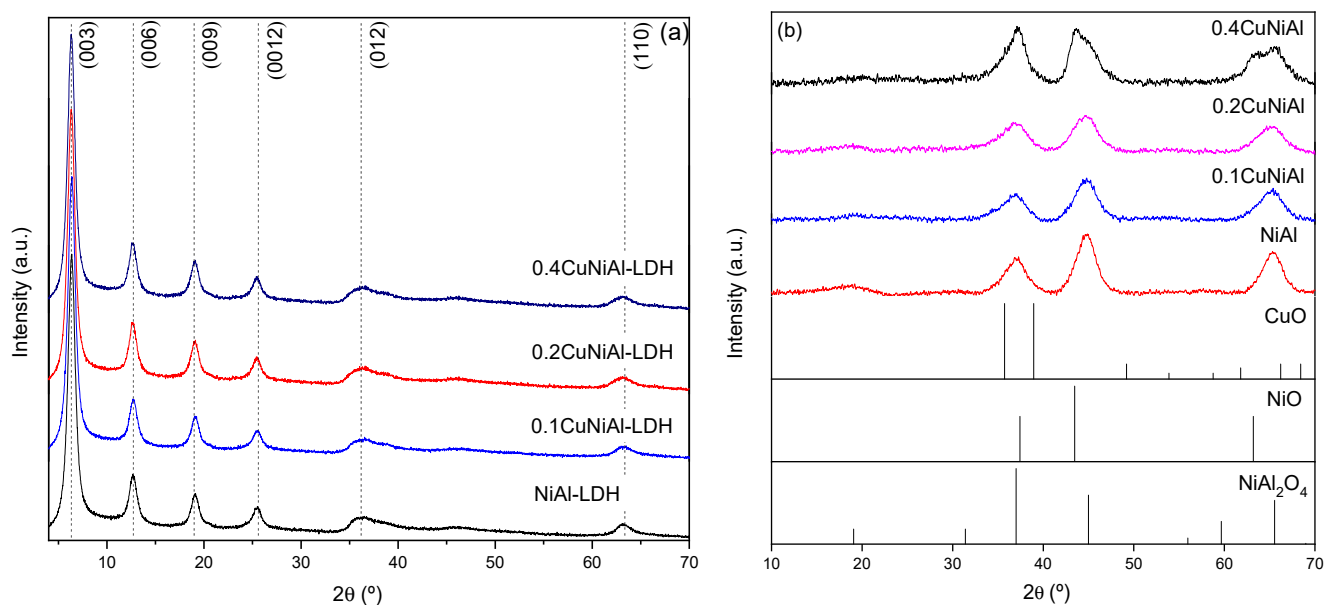
Sample	Ni (%)	Cu (%)	Al (%)	Theoretical Molar Ratios		Experimental Molar Ratios	
				$x$	Cu/Ni	$x$	Cu/Ni
NiAl	60.3	---	39.7	0.70	---	0.59	---
0.1CuNiAl	55.3	6.5	38.2	0.70	0.10	0.58	0.11
0.2CuNiAl	50.5	11.5	38.0	0.70	0.20	0.57	0.21
0.4CuNiAl	44.1	20.5	35.3	0.70	0.40	0.55	0.43

The X-ray diffraction patterns of the LDH-like precursors are illustrated in Figure 1a. In all samples, patterns of crystalline materials with reflections characteristic of LDH-type compounds were identified. The four intense and well-defined peaks present at angles  $2\theta < 30^\circ$  correspond to the basal distances of the planes (003), (006), (009) and (0012) [54,55]. Further, the two wider and less intense peaks at higher angles ( $2\theta > 30^\circ$ ) are also characteristic of LDHs, corresponding to (012) and (110) reflections [54,55]. It is important to note that the presence of segregated copper or aluminum phases was not found in the diffractograms of the CuNiAl LDHs, which demonstrates that the method used, with a theoretical Cu/Ni ratio  $\leq 0.4$ , was effective in obtaining LDH-type compounds containing Cu. This was despite the Jahn–Teller effect present in Cu LHDs, which consists of the spontaneous deformation of the octahedral geometry, hindering the formation of a pure and organized phase [56,57].

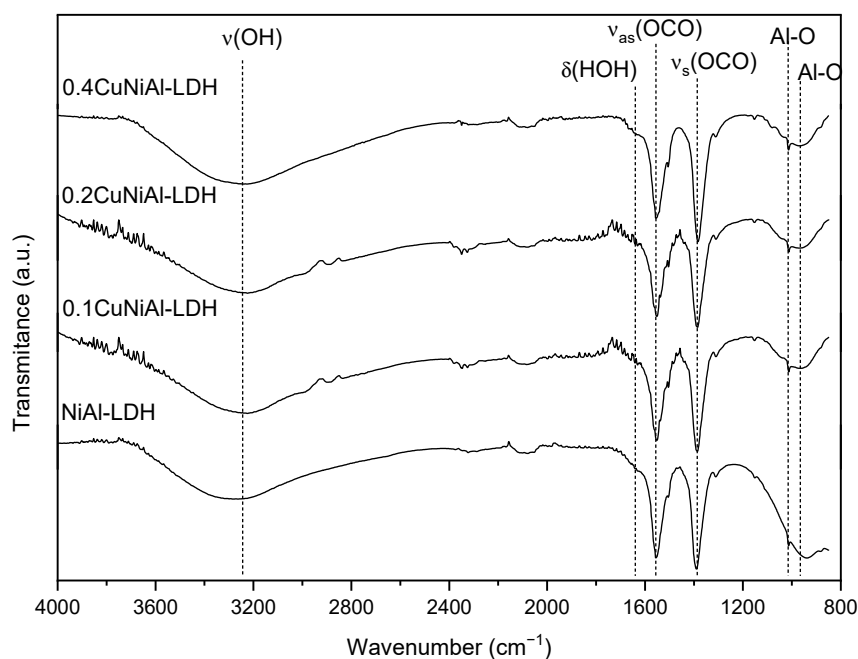
The basal distance  $c'$ , that is defined as the interlamellar distance plus the thickness of the brucite-type sheet, was calculated by the equation  $c' = d(003) = 2d(006) = 3d(009) = 4d(0012)$  [44,58]. In all samples, the basal distance assumed similar values, within the 13.9–14.0 Å range, as shown in Table S1. With an estimated thickness of 4.8 Å for the brucite-like sheet [59], the interlamellar distance calculated for all samples assumes values close to 9.1 Å, evidencing the formation of an LDH-type structure with terephthalate as the compensating anion, considering that the approximate value of its length is 9 Å [60–62].

Figure 2 shows the FTIR spectra of the precursors. The intense bands at 1555 and 1390 cm<sup>-1</sup> are assigned to stretching vibrations of carboxyl groups COO<sup>-</sup> from the terephthalate anion [54,57,60]. FTIR spectra also show bands related to the typical structure of LDHs. The band at 3250 cm<sup>-1</sup> refers to the  $\nu(\text{OH})$  stretching vibrations of the interlayer water and hydroxyls present in the LDHs sheets [54,60]. The band at 1640 cm<sup>-1</sup> is related

to interlayer water molecules angular deformation  $\delta(\text{H-O-H})$  [54,60], and the vibrations between  $1010$  and  $960\text{ cm}^{-1}$  refer to the Al-O bonds in octahedral  $\text{AlO}_6$  units [44].



**Figure 1.** XRD patterns of the NiAl and CuNiAl (a) LDH precursors and (b) mixed-oxide catalysts.



**Figure 2.** FTIR spectra of the NiAl and CuNiAl LDHs.

Thermogravimetric analysis results of the LDHs are shown in Figure 3. The curves indicate that the mixed oxides generated by the thermal treatment had thermal stability at temperatures above  $500\text{ }^{\circ}\text{C}$ . In all samples, the presence of three distinct stages of mass loss is observed, as reported in the literature [60]: the first is assigned to the loss of adsorbed water located in the interlamellar region ( $T < 175\text{ }^{\circ}\text{C}$ ); the second refers to the dehydroxylation of the brucite-like layers ( $175\text{ }^{\circ}\text{C} < T < 350\text{ }^{\circ}\text{C}$ ) and the third stage is assigned to the decomposition and combustion of terephthalate anions ( $350\text{ }^{\circ}\text{C} < T < 500\text{ }^{\circ}\text{C}$ ).

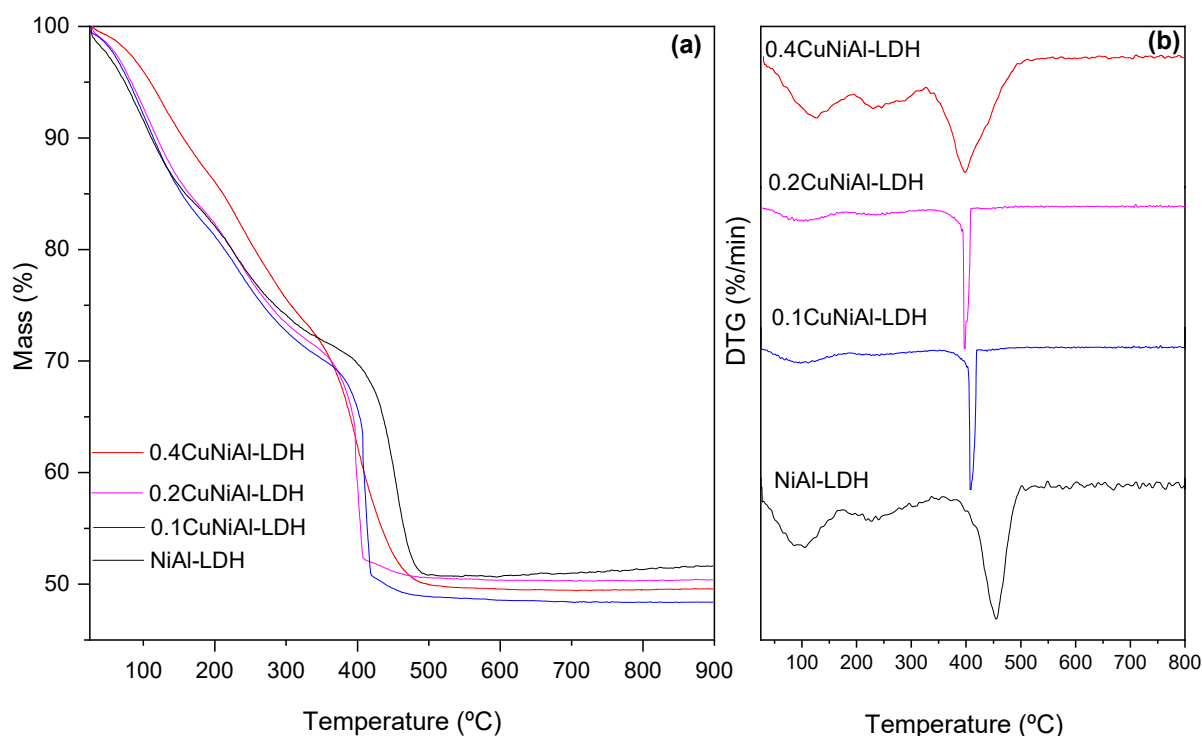


**Figure 3.** (a) Thermogravimetric analysis and (b) derivative curves of the NiAl and CuNiAl LDHs.

The total mass losses were 48.8%, 51.6%, 49.7% and 50.4% for NiAl-LDH, 0.1CuNiAl-LDH, 0.2CuNiAl-LDH and 0.4CuNiAl-LDH samples, respectively. The experimental results presented a less than 6.3% difference in relation to the theoretical mass loss values (Table S2). For calculating the theoretical mass loss (%) of the LDH-type precursors, the formula  $[(\text{Ni} + \text{Cu})_{1-x}\text{Al}_x(\text{OH})_2]^{x+}[\text{C}_8\text{H}_4\text{O}_4^{2-}]_{x/2} \cdot m\text{H}_2\text{O}$ , in which  $m = 1 - (3/2)x + 0.125$ , was used. The TGA curves also show that the maximum rate of mass loss, referring to the decomposition and combustion of terephthalate anions, differed between the precursors. While in the NiAl-LDH sample the maximum loss is at  $T = 454^\circ\text{C}$ , in the 0.1CuNiAl-LDH, 0.2CuNiAl-LDH and 0.4CuNiAl-LDH samples these events are at  $408^\circ\text{C}$ ,  $397^\circ\text{C}$  and  $398^\circ\text{C}$ , respectively, evidencing the action of Cu as a catalyst in the combustion of terephthalate anion [63].

Figure 1b shows the XRD of the mixed-oxide catalysts obtained by calcination of their LDH-type precursors at  $500^\circ\text{C}$ . Crystalline phases were identified by comparison with Inorganic Crystal Structure Database (ICSD) standards. In all samples, reflections related to a poorly crystallized  $\text{NiAl}_2\text{O}_4$  phase (ICSD-247071) were identified. It was possible to observe mixing with the NiO phase (ICSD-76670) in the 0.4CuNiAl sample through the overlapping of peaks around  $2\theta = 44^\circ$  and  $64^\circ$ . The reflection peak at  $2\theta = 37^\circ$  was used in Table 2 to calculate the average crystallite size of the  $\text{NiAl}_2\text{O}_4$  phase.

**Table 2.** Results of the NiAl and CuNiAl mixed-oxide catalysts textural analysis.

Sample	Surface Area ( $\text{m}^2 \text{g}^{-1}$ ) <sup>a</sup>	Average Pore Diameter ( $\text{\AA}$ ) <sup>b</sup>	Pore Volume ( $\text{cm}^3 \text{g}^{-1}$ ) <sup>b</sup>	$\text{NiAl}_2\text{O}_4$ Average Crystallite Size (nm) <sup>c</sup>
NiAl	230	100	0.65	2.9
0.1CuNiAl	272	85	0.67	2.7
0.2CuNiAl	253	77	0.54	2.4
0.4CuNiAl	262	55	0.40	2.9

<sup>a</sup> Calculated using the BET method; <sup>b</sup> Calculated using the BJH method; <sup>c</sup> Calculated by the Scherrer equation using the reflection peak at  $2\theta = 37^\circ$ .

No reflection peaks related to CuO (ICSD-16025) were identified in samples of Cu-NiAl mixed oxides, indicating that this phase was present in the amorphous form or with very small crystallite sizes. The calcination temperature chosen may also have been insufficient to identify other possible crystalline phases, such as  $\text{Al}_2\text{O}_3$ , which is possibly present in the amorphous form and can contribute to the high surface area of the catalysts. Lopes et al. [57] reported that increasing the calcination temperature of LDHs led to increased crystallinity but severely reduced the catalysts' surface area.

Table 2 shows that the NiAl catalyst had a total specific area of  $230 \text{ m}^2 \text{ g}^{-1}$ . The addition of copper, in turn, increased the specific area to the range of  $253\text{--}272 \text{ m}^2 \text{ g}^{-1}$ . These values were higher than the specific areas reported in CuNiAl and NiAl mixed oxides derived from LDHs containing carbonate as a compensating anion [64–66].

Figure 4 shows the adsorption–desorption isotherms and pore size distribution of the NiAl and CuNiAl mixed oxides. Type IV isotherms with H3 hysteresis loops were observed in all catalysts, according to IUPAC classification. These isotherms are characteristic of mesoporous solids and the hysteresis loop results from capillary condensation inside the pores [67]. This classification agrees with reports in the literature about mixed oxides derived from NiAl and CuNiAl LDH precursors containing terephthalate as a compensating anion [38,57]. There are observable differences between the isotherms, caused by the addition of copper, such as a decrease in the amount of  $\text{N}_2$  ( $\text{cm}^3/\text{g}$ ) adsorbed at higher partial pressures ( $P/P_0$ ) and a significant narrowing in the hysteresis loop of the 0.4CuNiAl catalyst, resulting in smaller average pore diameter values, in all CuNiAl oxides, and a smaller average pore volume in the 0.2CuNiAl and 0.4CuNiAl samples, as observed in Table 2, which is also reflected in the pore distribution curves, inserted in Figure 4.

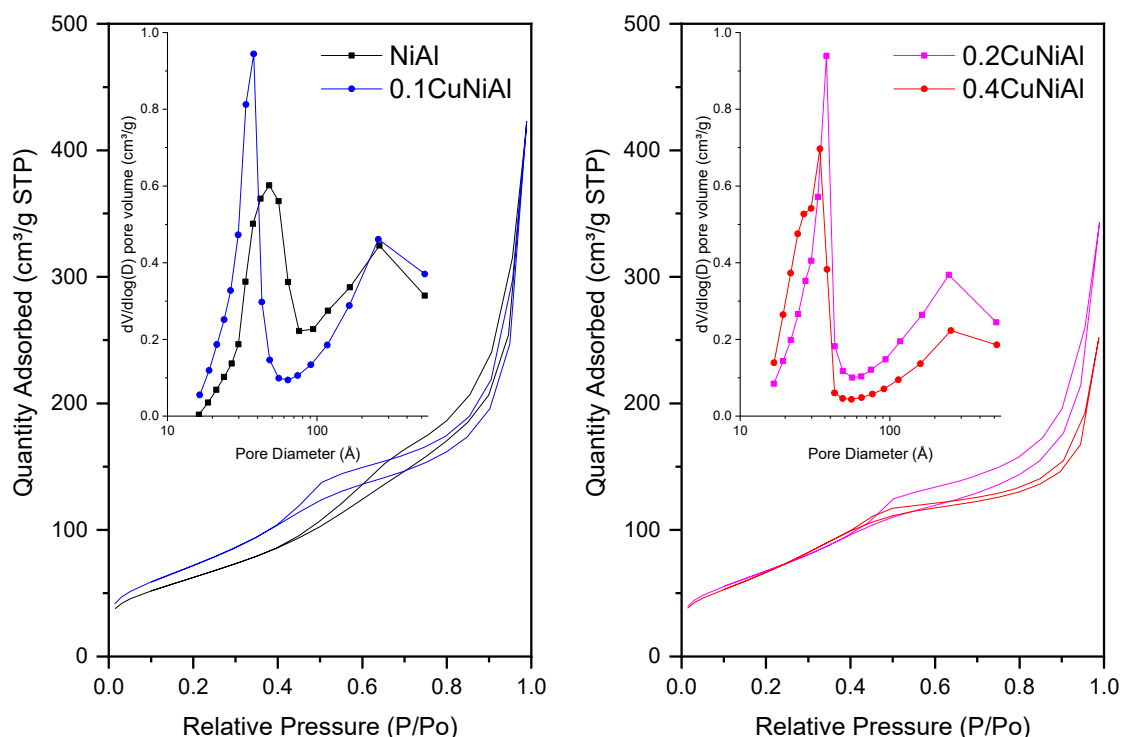


**Figure 4.** Nitrogen sorption isotherms and pore size distribution (inserted) of the NiAl and CuNiAl mixed-oxide catalysts.

Figure 5 shows the temperature-programmed reduction (TPR) profiles of the mixed oxides. The NiAl catalyst reduction curve showed two overlapping stages related to nickel reduction, between  $380 \text{ }^\circ\text{C}$  and  $840 \text{ }^\circ\text{C}$ . The occurrence of these two steps is related to the strength of the interaction between Ni and Al [68,69]. The first stage, with maximum  $\text{H}_2$  consumption at  $420 \text{ }^\circ\text{C}$ , represents the reduction of Ni whose interaction with Al is weak.

The second stage, with maximum consumption at 598 °C, represents the reduction of Ni whose interaction is stronger. The larger area of this last step is related to a higher H<sub>2</sub> consumption, which indicates that the nature of the Ni–Al interactions was predominantly strong. The Cu addition shifted the high temperature events towards lower temperatures, which demonstrates a decrease in the Ni–Al interaction strength, with consequently greater reducibility. This effect is justified by the proximity of Ni and Cu in the brucite-like sheets of the LDH precursors [70], since, according to the literature, the synergistic interaction between Ni and Cu contributes to the reducible properties of these metals [66,70].

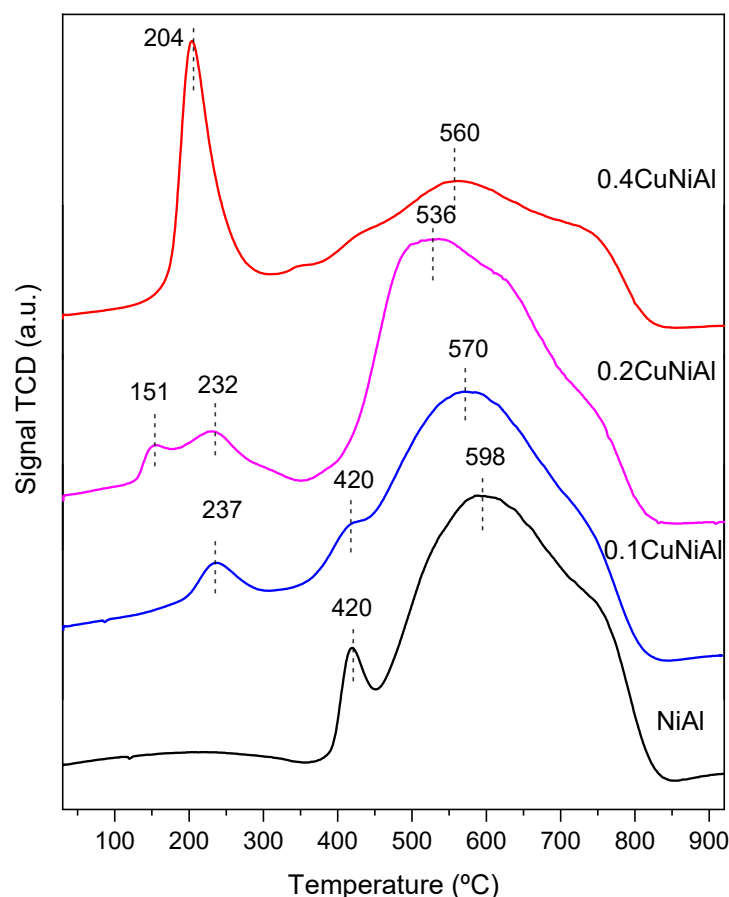


**Figure 5.** Temperature-programmed reduction (TPR) curves of the NiAl and CuNiAl mixed-oxide catalysts.

Regarding the copper oxide reduction in CuNiAl catalysts, the presence of one or two stages of H<sub>2</sub> consumption at lower temperatures is noted (130 °C–340 °C) [57,65,70], and it is not possible to observe profiles that indicate the existence of Cu–Ni alloys. Specifically, in the 0.2CuNiAl catalyst, there are two stages of CuO reduction, with maximum H<sub>2</sub> consumption at 151 °C and 232 °C. The first stage is possibly associated with the reduction of more dispersed CuO particles and the second with larger CuO particles [65]. Another possibility would be the occurrence of a progressive reduction from Cu<sup>2+</sup> to Cu<sup>+</sup> and Cu<sup>+</sup> to Cu<sup>0</sup> [57].

### 3.2. Oleic Acid Pyrolysis

The total ion chromatograms of oleic acid pyrolysis, both pure and adsorbed on NiAl and CuNiAl mixed oxides, are shown in Figure 6. The results show that the mixed-oxide catalysts were efficient in the complete conversion of oleic acid (OA), considering the peak attributed to OA in 51.4 min. The addition of NiAl and CuNiAl catalysts also promoted the formation of a greater variety of compounds, when compared to the pyrolysis of pure oleic acid.

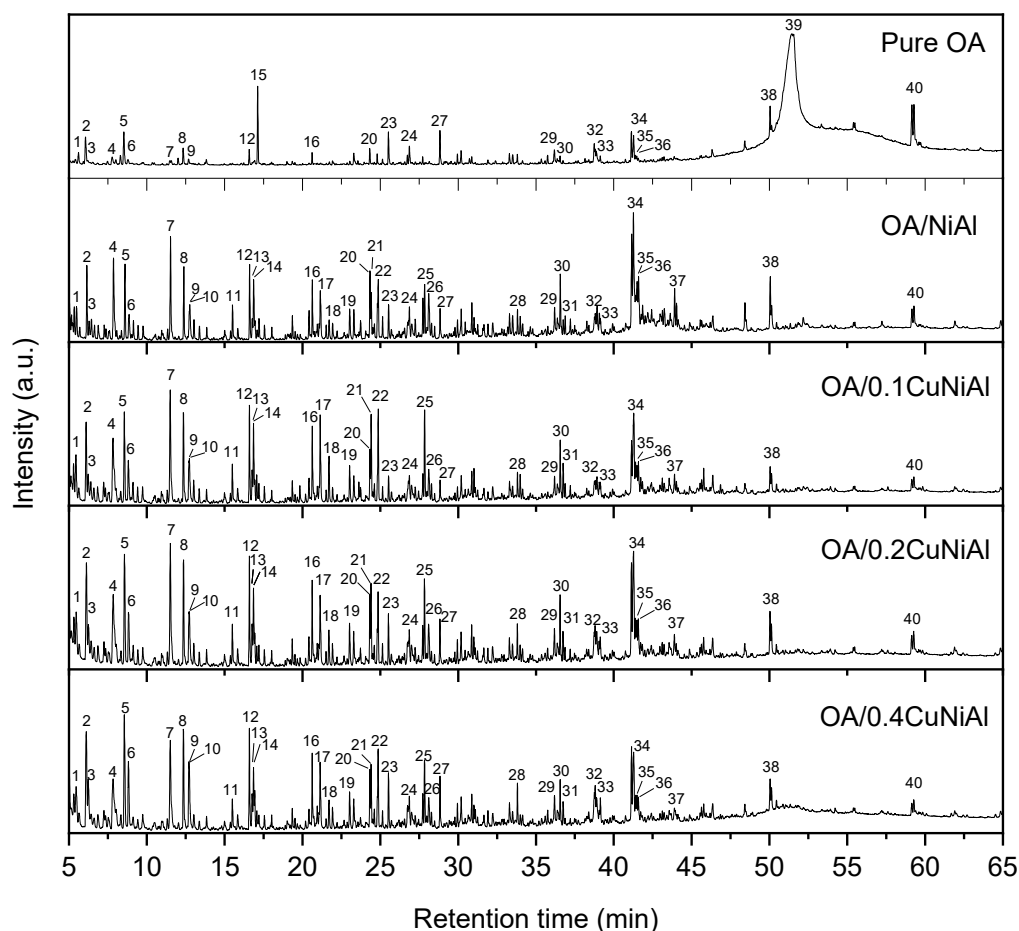


**Figure 6.** Total ion chromatograms from the fast pyrolysis of oleic acid (OA), pure and in presence of catalyst, at 550 °C. Main compounds identified: (1) 1,3-cyclopentadiene, (2) 1-hexene, (3) *n*-hexane, (4) benzene, (5) 1-heptene, (6) heptane, (7) toluene, (8) 1-octene, (9) octane, (10) hexanal, (11) ethylbenzene, (12) 1-nonene, (13) styrene, (14) *o*-xylene, (15) cyclohexane, ethenyl-, (16) 1-decene, (17) octanal, (18) cyclopentanone, (19) indene, (20) 1-undecene, (21) 2-nonanone, (22) nonanal, (23) 1,4-undecadiene, (24) benzene, pentyl-, (25) 2-decanone, (26) naphthalene, (27) 8-dodecen-1-ol, (28) 1-tetradecene, (29) benzene, octyl-, (30) 1-pentadecene, (31) pentadecane, (32) 1,7-hexadecadiene, (33) benzene, nonyl-, (34) 8-heptadecene, (35) benzene, decyl-, (36) *n*-heptadecanol-1, (37) benzene, undecyl-, (38) 9-octadecenal, (39) oleic acid, (40) oleyl acetate.

8-Heptadecene appears as one of the main products in all pyrograms, indicating that decarboxylation and decarbonylation reactions are among the main OA conversion routes in the fast pyrolysis at 550 °C. This conclusion is reinforced by the fact that CO<sub>2</sub> was the compound with the largest area in the catalytic pyrolysis (r.t. 4.2 min), not shown in Figure 6 due to its high relative intensity. Regarding products with retention times shorter than 5 min, propene and 2-butene were also formed in large quantities and their area percentages increased significantly with the use of catalysts, indicating acceleration of the cracking reactions. In addition to 8-heptadecene, several C<sub>5</sub>+ alkenes, mostly linear, were identified in all pyrograms; the main ones were 1-pentene, 1-hexene, 1-heptene, 1-octene and 1-nonene, in agreement with previous studies on fatty acid pyrolysis reported in the literature [44,71]. No peaks related to C<sub>18</sub> alkenes or alkanes were found, reinforcing evidence of the occurrence of decarboxylation/decarbonylation reactions.

The aromatics toluene and benzene were among the top ten products formed in all catalytic reactions; however, they were not observed in pure oleic acid pyrolysis. Other aromatics, such as *o*-xylene and naphthalene, also showed a significant area percentage in catalytic reactions. Further, a homologous series of linear alkylbenzenes was identified,

starting from toluene (C7) to undecylbenzene (C17). These results align with those reported in previous pyrolysis studies using mixed oxides containing NiAl [38,44]. In Figure 6, oxygenated compounds are also identified. Among the aldehydes, mainly small molecules were formed, such as octanal and nonanal, but 9-octadecenal was also among the main identified products. Cycloheptanone, 2-nonanone and 2-decanone were among the main identified ketones. Among the alcohols, 8-dodecen-1-ol and 1-heptadecanol were formed in greater quantity. Oleyl acetate was another oxygenate identified, formed in lower quantity in the catalytic reactions.

Figure 7 shows the product distribution of oleic acid pyrolysis, pure or adsorbed on mixed-oxide catalysts, grouped into five categories: CO<sub>2</sub>, hydrocarbons, oxygenates, unidentified compounds and untransformed oleic acid. Non-catalytic pyrolysis resulted in ~49% conversion of oleic acid; however, in the presence of NiAl and CuNiAl catalysts, the conversion was complete. Previous studies have demonstrated the efficiency of catalysts containing Ni, Cu or Al in the conversion of various fatty acids [39,44,71], due to the high activity of Ni in C–C cracking reactions [39] and the promotion of decarbonylation/decarboxylation reactions by copper [47], as well as hydrogen transfer and deoxygenation mechanisms related to the Lewis acid sites of alumina [72].

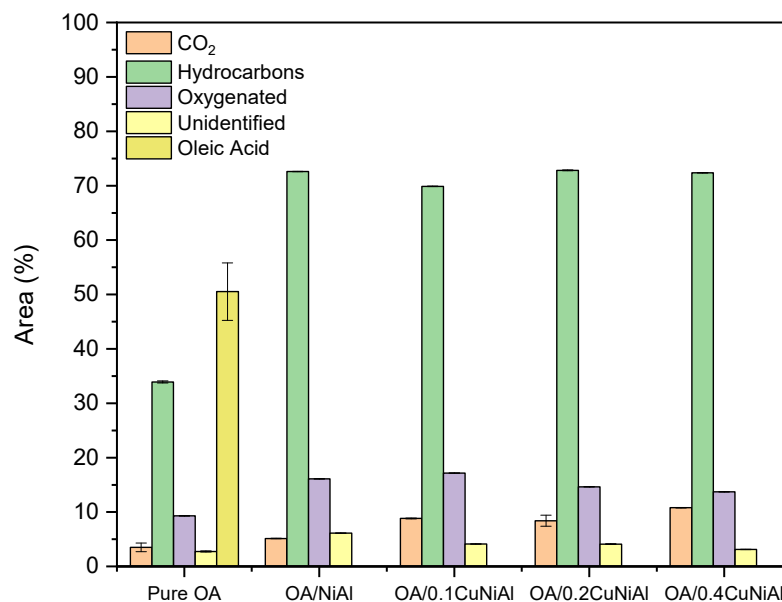


**Figure 7.** Product distribution from the pyrolysis at 550 °C of oleic acid (OA), pure and in presence of NiAl and CuNiAl mixed oxides.

There was no significant difference between the catalysts in the total amount of hydrocarbons formed. However, the addition of Cu to the catalytic composition promoted less formation of unidentified compounds, as well as a notable increase in the formation of CO<sub>2</sub>. Studies in the literature have reported that the association of Ni and Cu contributes to increased decarboxylation ability [39,47]. Thus, the increase in CO<sub>2</sub> formation by the CuNiAl catalysts is related to a greater activity of oleic acid decarboxylation, which contributed to the lower formation of oxygenates promoted by the 0.4CuNiAl catalyst. These results are in line with those previously reported, which have indicated an increase in the degree of deoxygenation with CuNi catalysts in oleic acid conversion [39,47].

The distribution of hydrocarbons by carbon chain length is shown in Figure 8, with the following classification: C3–C4 (gaseous), C5–C9 (gasoline), C10–C13 (kerosene) and C14+ (diesel). The significant formation of hydrocarbons in the C5–C9 range suggests preferential cracking near the C=C bond, as reported by Santos et al. [71]. When comparing the catalysts, the formation of light gases and hydrocarbons in the gasoline range was favored by the CuNiAl catalysts, compared with the catalyst containing only NiAl. However, there was a

decrease in the formation of hydrocarbons in the C10–C13 and C14+ range, thus indicating a favoring of the C–C bonds in cracking reactions. Previous studies have demonstrated that the formation of Cu–Ni alloys disfavors C–C scissions in nickel catalysts [47]; the addition of copper to the mixed oxides in the present study, however, showed the opposite effect. The increase in C–C cracking reactions can be explained by an increase in the presence of uncombined nickel in the catalysts, possibly induced by copper addition. As observed in Figure 5, the addition of copper in the synthesis of mixed oxides decreased the Ni–Al interaction. This effect may indicate the occurrence of competitive interaction of copper with  $\text{AlO}_x$  species, releasing uncombined Ni. These nickel species would then be responsible for increasing the cracking power of the catalysts.

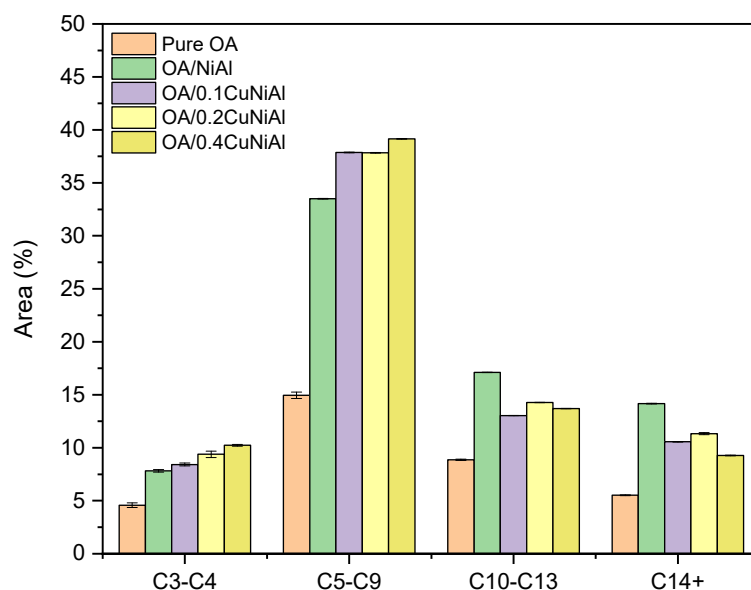


**Figure 8.** Carbon chain length distribution of hydrocarbons from the pyrolysis at 550 °C of oleic acid (OA), pure and in presence of NiAl and CuNiAl mixed oxides.

The distribution of hydrocarbon families is detailed in Figure 9. Most monoalkenes were formed. There was also the formation of alkanes, polyunsaturated and aromatic hydrocarbons. Dienes were the main polyunsaturated compounds obtained. Among the aromatic compounds, monoaromatics were the majority compared to polyaromatics. The presence of aromatic compounds among the main products implies the occurrence of dehydrogenation reactions, which have been reported in catalysts based on Ni and CuNi oxides [39,44,73].

In turn, the generation of endogenous  $\text{H}_2$  can promote hydrogenation reactions, even under inert atmosphere conditions [39,73]. Zhang et al. [47] reported that the addition of Cu to Ni catalysts increased the in situ hydrogenation of oleic acid. This result agrees with the present study, where a greater formation of alkanes was observed with the addition of Cu to the NiAl catalysts (Figure 9). Among the catalysts, an increase in Cu content also promoted less formation of monoaromatic and polyaromatic hydrocarbons, leading to a decrease in the Aromatic/Non-Aromatic ratio from 0.51 to 0.33. Specifically, the lower formation of polyaromatics indicates copper action in inhibiting catalytic deactivation, considering that these compounds are precursors of coke [74]. The positive effect of Cu on coke inhibition is in line with previous results reported in the literature [39].

In Table 3, alkenes and alkanes formed during the pyrolysis reaction are classified as linear, cyclic or ramified. Linear hydrocarbons were formed in greater quantity and their origin, in most part, comes from C–C cracking reactions of alkyl chains from oleic acid and primary products of its conversion [75]. Table 3 also shows that cycloalkenes and ramified alkenes were formed in small amounts.

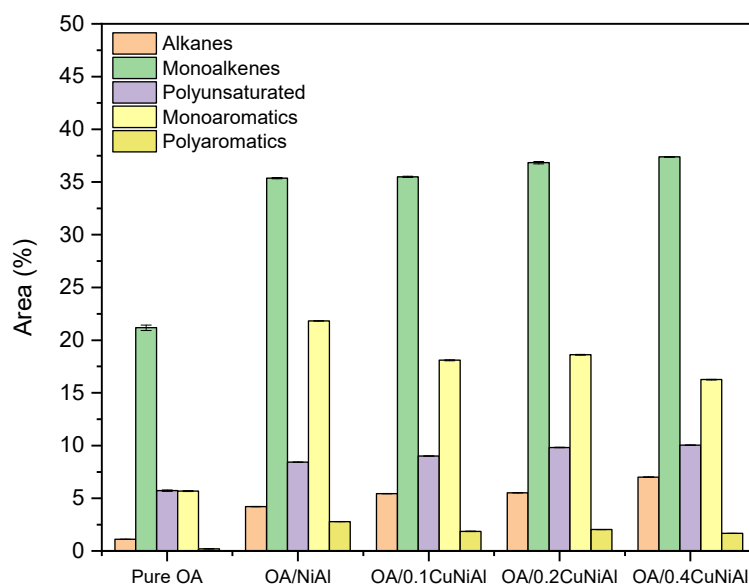


**Figure 9.** Hydrocarbon family distribution from the pyrolysis at 550 °C of oleic acid (OA), pure and in presence of NiAl and CuNiAl mixed oxides.

**Table 3.** Distribution of alkanes and alkenes from the pyrolysis at 550 °C of oleic acid (OA), pure and in presence of NiAl and CuNiAl mixed oxides, according to their families.

Catalyst	Linear Alkanes	Linear Alkenes	Cycloalkene	Ramified Alkenes
Pure Oleic Acid	1.12	20.63	6.28	---
NiAl	4.21	40.67	2.29	0.82
0.1CuNiAl	5.45	39.92	3.24	1.33
0.2CuNiAl	5.52	42.15	3.29	1.22
0.4CuNiAl	7.01	42.96	3.49	0.97

Figure 10 shows the distribution of oxygenated compounds based on their functional groups. Esters were the main oxygenated products obtained in the absence of catalyst. In turn, the catalysts preferentially promoted the formation of alcohols, aldehydes and ketones. The formation of ketones was identified only in catalytic reactions, which is related to the catalytic activity of alumina [72]. Compared to the NiAl catalyst, the CuNiAl catalysts preferentially promoted the formation of ketones and aldehydes compared to alcohol, as well as less formation of esters. It is important to note that CuNi association preferentially promoted the formation of C6–C10 oxygenated compounds, indicating deep C–C cracking of the alkyl chains, which is related to the increased presence of uncombined nickel.

### 3.3. Reaction Pathways

Based on the main products formed in the catalytic pyrolysis and on data from the literature, Figure 11 sets the oleic acid pyrolysis mechanism at 550 °C with NiAl and CuNiAl mixed-oxide catalysts. As previously mentioned, the presence of CO<sub>2</sub> and 8-heptadecene among the main products indicates the occurrence of oleic acid decarboxylation (Equation (1)) [73]. 8-Heptadecene underwent isomerization and cracking, preferably close to the C=C bond [71], forming alkenes with a lower carbon number (Equation (2a)). Further cracking reactions resulted in the formation of light gases (Equation (2b)). In addition to beta scission, forming two alkenes (Equations (2a) and (2b)), alkene cracking reactions also resulted in the formation of alkanes and dienes (Equation (3)) [44]. Part of the dienes formed were combined with alkenes through a Diels–Alder mechanism, generating cycloalkenes (Equation (4)) [76–78]. Subsequently, these compounds underwent dehydrogenation steps to form aromatics [77,78] (Equation (5)).

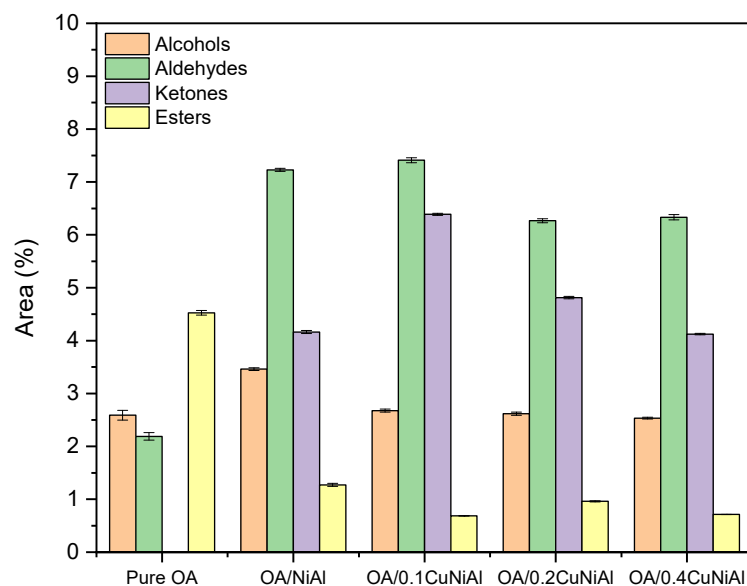


**Figure 10.** Distribution of oxygenated products from the pyrolysis at 550 °C of oleic acid (OA), pure and in presence of NiAl and CuNiAl mixed oxides.

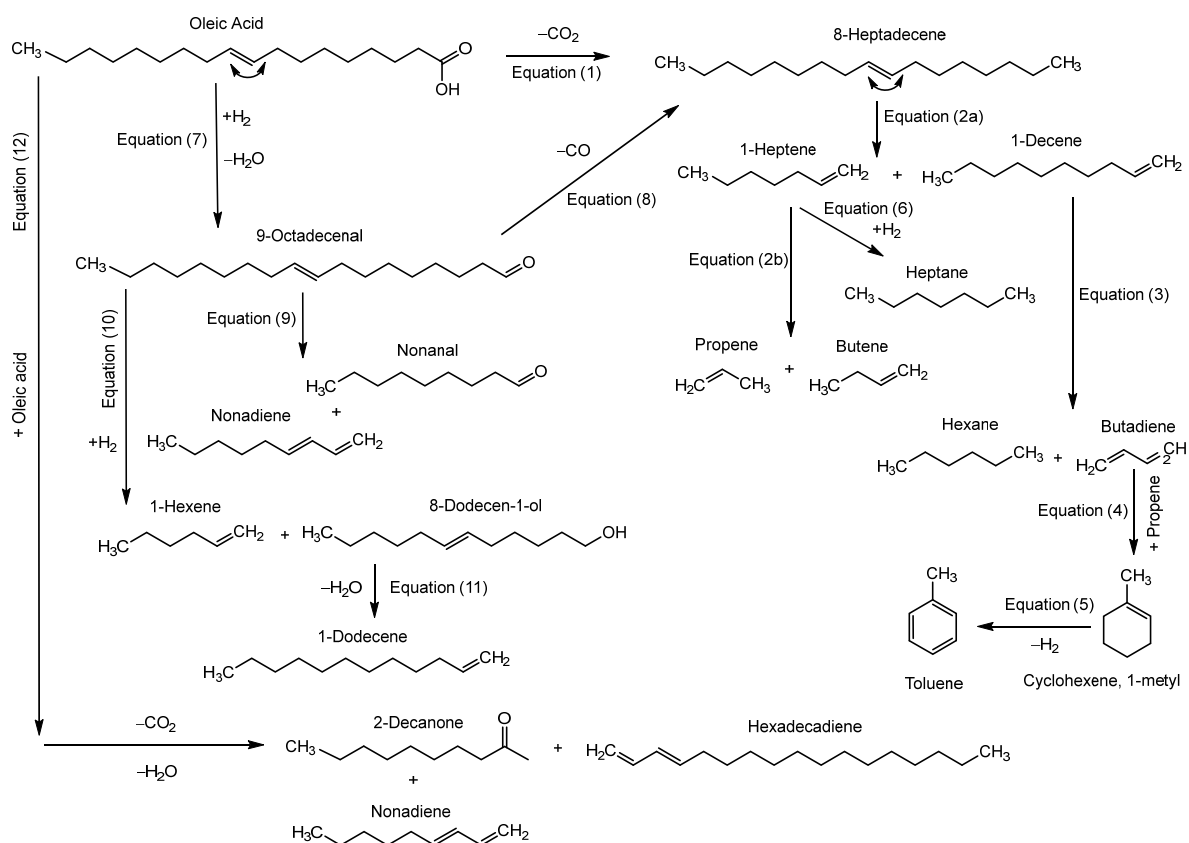


**Figure 11.** Proposed reaction mechanism for the pyrolysis of oleic acid on NiAl and CuNiAl mixed oxides, at 550 °C.

Endogenous hydrogen, from the dehydrogenation and aromatization reactions, was used in hydrogenation reactions [39,73], promoting greater formation of alkanes (Equation (6)). In turn, the formation of 9-octadecenal was promoted by oleic acid reduction (Equation (7)) through a mechanism that includes the chemisorption of carbonyl oxygen at the Lewis acid sites of alumina ( $\text{Al}_2\text{O}_3$ ), present on the catalyst surface [72,79].

Decarbonylation reactions of aldehydes, such as 9-octadecenal (Equation (8)), were another possible route for hydrocarbon generation [80]. As the aldehydes formed in the catalytic pyrolysis reactions were mostly C6–C9, the occurrence of C–C cracking reactions of the alkyl chains was presumed (Equation (9)). Part of the aldehydes formed also underwent hydrogenation reactions, forming alcohols (Equation (10)) [80]. Due to the reaction conditions, a portion of the generated alcohols underwent dehydration (Equation (11)) [79]. The formation of ketones occurred through a ketonization route of carboxylic acids, promoted by alumina, which comprises the formation of symmetrical ketones and subsequent conversion into methyl ketones through a hydrogen transfer mechanism [72,81]. The presence of 1,7-hexadecadiene among the major products is the main evidence for the occurrence of this mechanism. As the main ketones identified were in the C7–C10 range, the occurrence of C–C cracking of the alkyl chains of the intermediate ketones involved in this mechanism was also indicated, as summarized in Equation (12).

In summary, the cracking reactions of alkyl chains of compounds derived from oleic acid (Equations (2), (3), (9) and (12)) led to the formation of large amounts of linear hydrocarbons. Lewis acid sites of alumina ( $\text{Al}_2\text{O}_3$ ) favored hydrogen transfer (Equation (7)) and ketonization (Equation (12)) mechanisms. In turn, the higher presence of uncombined Ni, promoted by the addition of Cu to the catalysts, favored hydrogenation (Equations (6) and (7)) and cracking (Equations (2), (3) and (9)) reactions, as well as deoxygenation reactions (Equations (1), (8), (11) and (12)), contributing to the increase in the formation of short chain alkanes and alkenes (C3–C9), as well as a lower content of oxygenates. However, aromatization reactions (Equation (5)) were unfavored by increasing copper content.

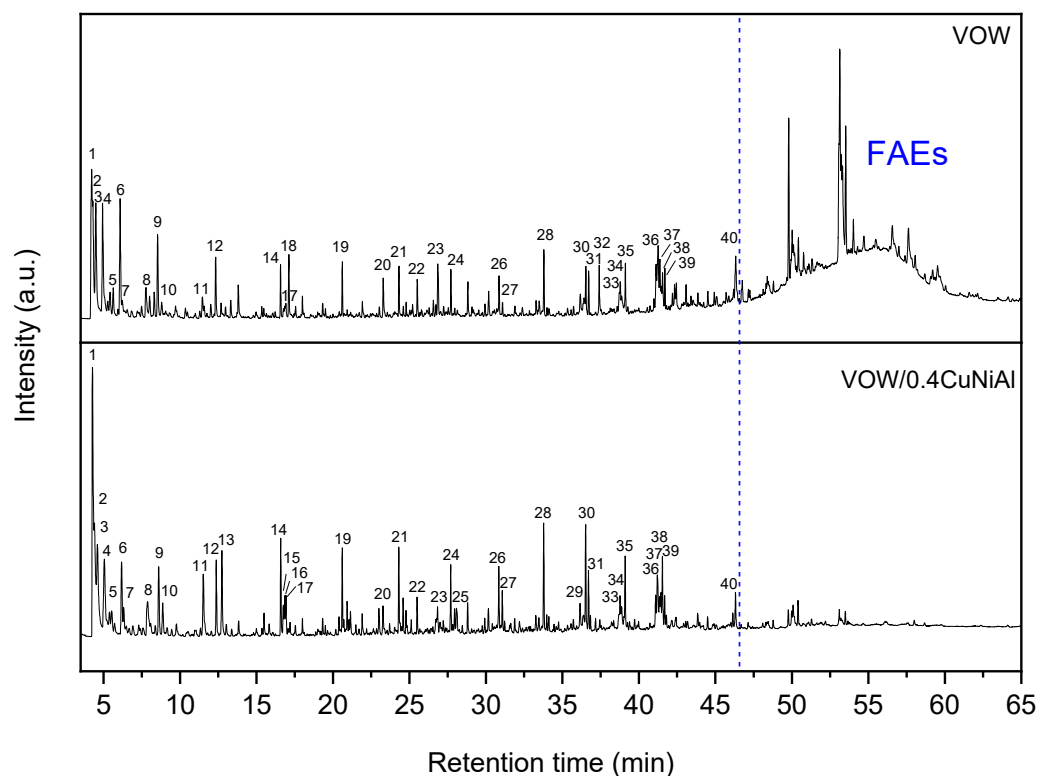
### 3.4. Vegetable Oil Waste Pyrolysis

Total ion chromatograms of thermal and thermocatalytic pyrolysis of vegetable oil waste (VOW) at 550 °C are shown in Figure 12. An industrial vegetable oil residue with a large amount of free fatty acids (FFA) and triglycerides was used. The 0.4CuNiAl catalyst was chosen because it promoted greater deoxygenation in the oleic acid pyrolysis (Figure 7), as well as less formation of coke precursors (Figure 9). Compared to thermal pyrolysis, the catalyst promoted a significant increase in the conversion of compounds present at retention times greater than 46.5 min. This region of the chromatogram contains a high concentration of fatty acid esters (FAEs) and unidentified compounds, linked to the complex composition of VOW, as well as some ketones and C17+ aldehydes. Consequently, the thermocatalytic reaction promoted the formation of a greater variety of products, with higher relative intensity, which shows the positive effect of the catalyst on the reaction.

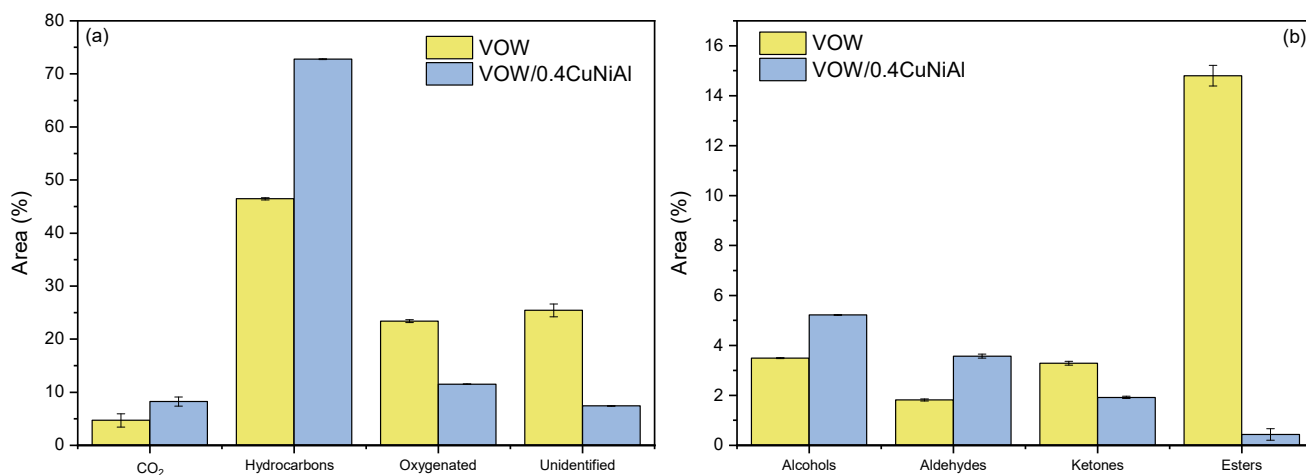
Similar to what had been observed in the oleic acid pyrolysis, a series of homologous peaks related to 1-alkenes was identified in both pyrograms, comprising mainly short-chain 1-alkenes, such as 1-hexene, 1-heptene and 1-octene. 1-Heptadecene was the alkene with the highest number of carbons obtained. In the catalytic pyrolysis, a greater amount of aromatic compounds was identified, especially toluene, benzene and *o*-xylene, as well as a homologous series of linear alkylbenzenes, starting from toluene (C7) to dodecylbenzene (C18). In addition to the FAEs identified at r.t. > 46.5 min, several oxygenated compounds with shorter retention times were identified in both pyrograms, especially hexanal, 1-heptadecanol and 1-hexadecanol, as well as 2-hexadecanone in thermocatalytic pyrolysis and methyl dodecanoate ester, which was identified only in thermal pyrolysis.

Figure 13a shows the distribution of the compounds from the VOW pyrolysis. The catalyst promoted a significant increase in hydrocarbons and  $\text{CO}_2$  formation, as well as a sharp decrease in oxygenates and unidentified compounds, indicating a significant increase in the conversion of substrate components, as observed in the pyrograms (Figure 12, r.t. > 46.5 min). This effect is more evident in Figure 13b, which shows the distribution of the oxygenated compounds by functional groups. It is possible to observe a strong decrease in the content of esters, indicating the deoxygenating activity of the catalyst. The content of ketones also showed a decrease. However, the increase in the conversion of components

from VOW, in thermocatalytic pyrolysis, resulted in the increased formation of aldehydes and alcohols.



**Figure 12.** Total ion chromatograms from the fast pyrolysis of vegetable oil waste (VOW), pure and adsorbed on the 0.4CuNiAl catalyst, at 550 °C. Main compounds identified: (1) carbon dioxide, (2) propene, (3) 2-butene, (4) 1-pentene, (5) 1,3-cyclopentadiene; (6) 1-hexene, (7) *n*-hexane, (8) benzene, (9) 1-heptene, (10) heptane, (11) toluene, (12) 1-octene, (13) hexanal, (14) 1-nonene, (15) styrene, (16) *o*-xylene, (17) nonane, (18) cyclohexane, ethenyl-, (19) 1-decene, (20) benzene, *n*-butyl-, (21) 1-undecene, (22) 1,4-undecadiene, (23) benzene, pentyl-, (24) 1-dodecene, (25) naphthalene, (26) 1-tridecene, (27) tridecane, (28) 1-tetradecene, (29) benzene, octyl-, (30) 1-pentadecene, (31) pentadecane, (32) dodecanoic acid, methyl ester, (33) 1,7-hexadecadiene, (34) benzene, nonyl-, (35) 1-hexadecanol, (36) 1-heptadecene, (37) 3-heptadecene, (38) benzene, decyl-, (39) *n*-heptadecanol-1, (40) 2-hexadecanone. The dotted blue line at 46.5 min indicates the beginning of a fatty acid esters (FAEs) and unidentified compounds.



**Figure 13.** (a) Product distribution and (b) oxygenated compound distribution from the pyrolysis at 550 °C of vegetable oil waste (VOW), pure and in presence of the 0.4CuNiAl mixed oxide.

In Figure 14a, the hydrocarbons generated by VOW pyrolysis are classified according to their families. The greater conversion of VOW components by the 0.4CuNiAl catalyst promoted an increase in the formation of hydrocarbons in all families; this effect, however, was proportionally greater in the formation of alkanes and aromatics, indicating greater promotion of hydrogen transfer reactions. In Figure 14b, hydrocarbons are classified according to carbon chain length. As observed in the oleic acid pyrolysis (Figure 8), the 0.4CuNiAl catalyst favored the formation of hydrocarbons in the gasoline range. Another observed effect was the favoring of kerosene over diesel.

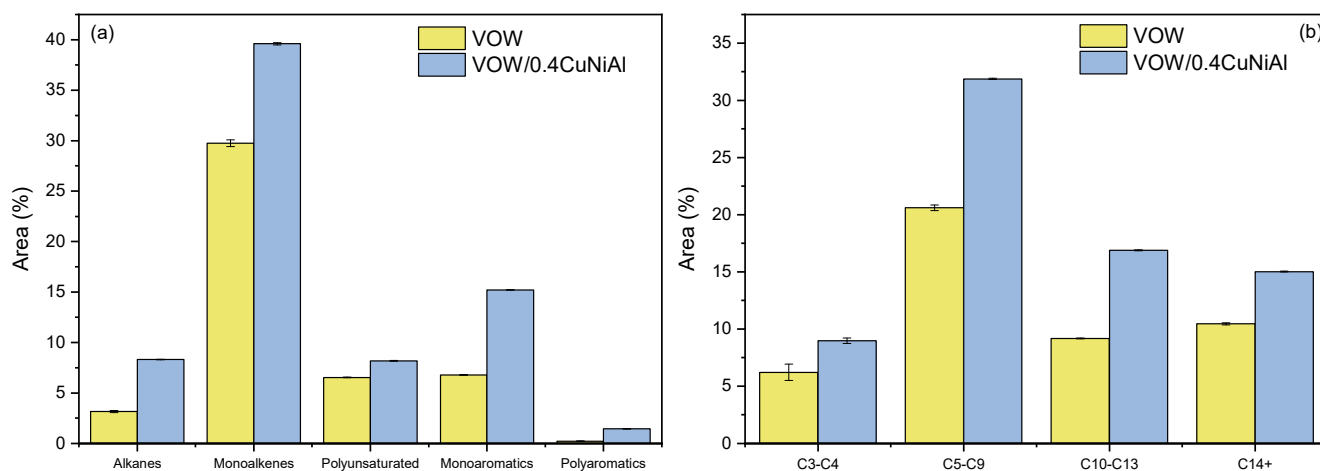


**Figure 14.** Hydrocarbon distribution from the pyrolysis at 550 °C of vegetable oil waste (VOW), pure and in presence of the 0.4CuNiAl mixed oxide, according to their (a) family and (b) carbon chain length.

#### 4. Discussion

The results of the present study provide novel information for the design of efficient catalysts for waste oil conversion into valuable deoxygenated products. The catalysts can be applied in biorefining processes for the production of syngas and second-generation biofuels through the pyrolysis of raw materials such as waste cooking oil and soapstocks [30,33]. The identification of a homologous series of linear alkylbenzenes, observed in catalytic pyrolysis, also points to a possible route for biosurfactant production. Regarding future research, the catalysts can be associated with other metals in order to evaluate the synergistic effects between the metallic species and increase the deoxygenation and hydrogenation activity. Based on the hydrogenating activity observed, pyrolysis studies in the presence of hydrogen can also be a route for converting vegetable oil waste, with a high degree of deoxygenation, using the CuNiAl mixed-oxide catalysts derived from LDHs.

#### 5. Conclusions

Through different characterization techniques, the effective formation of NiAl and CuNiAl precursors with an LDH-type structure, containing terephthalate as a compensation anion, was demonstrated. The mixed-oxide catalysts derived from these precursors showed a specific surface area between 230 and 272 m<sup>2</sup> g<sup>-1</sup> with NiAl<sub>2</sub>O<sub>4</sub> crystallite sizes between 2.4–2.9 nm. No Cu–Ni alloys were found; the addition of copper, however, promoted significant changes in the textural analyses of the materials, as well as in the TPR curves, indicating a weakening of the Ni–Al interaction and favoring the reduction of Ni.

The catalysts were efficient in the complete conversion of oleic acid (OA) by pyrolysis at 550 °C, in the absence of added hydrogen, compared to the 49% conversion obtained in the pyrolysis of pure OA. The main products of catalytic pyrolysis were linear alkenes and aromatic compounds such as benzene and toluene. The addition of copper to the synthesis of the mixed oxides favored the formation of uncombined nickel, promoting an increase in the cracking power of the CuNiAl catalysts when compared to the NiAl

catalyst, resulting in a greater formation of light gases and hydrocarbons in the range of gasoline. The presence of copper also promoted the activity of Ni in hydrogenation reactions, favoring the formation of alkanes; this increased the deoxygenation of oleic acid and reduced the formation of aromatics and coke precursors.

The application of the catalyst with Cu/Ni ratio of 0.4 in the pyrolysis of an industrial vegetable oil residue, high in free fatty acids and triglycerides, pointed to a strong catalytic activity in the conversion of the residue components. Compared to the pyrolysis of the pure residue, the catalytic pyrolysis promoted an accentuated decrease in the content of oxygenates and an increase in the hydrocarbons formation, mostly in the gasoline carbon range. The results showed that the CuNiAl mixed-oxide catalysts can be useful in the conversion of vegetable oil waste into deoxygenated products, as second-generation biofuels and also useful chemicals for biosurfactants precursors.

**Supplementary Materials:** The following supporting information can be downloaded at: <https://www.mdpi.com/article/10.3390/en16176131/s1>, Table S1: Calculated  $d$  values from the reflection peaks ( $2\theta < 30^\circ$ ) of the NiAl and CuNiAl LDHs; Table S2: Comparison between thermogravimetric analyses and theoretical mass loss percentage of the NiAl and CuNiAl LDHs.

**Author Contributions:** Conceptualization, J.S.; Methodology, J.S., D.O.L., J.F.G. and S.A.; Resources, J.G.A.P.; Writing—original draft, J.S. and J.G.A.P.; Writing—review and editing, S.A., F.R.C., C.M.B.M.B., I.C.L.B., R.F. and J.G.A.P.; Supervision, J.G.A.P.; Project administration, J.G.A.P.; Funding acquisition, J.G.A.P. All authors have read and agreed to the published version of the manuscript.

**Funding:** This research was funded by Coordination of Higher Education Personnel Improvement (CAPES) (grant number: 88882.306335/2018-01), Fundação de Amparo à Ciência e Tecnologia do Estado de Pernambuco (FACEPE) (grant numbers: IBPG-0395-3.06/19, BCT-0378-3.06/17 and APQ-0906-3.06/17), National Council for Scientific and Technological Development (CNPq) (grant numbers: 430921/2016-0, and 312387/2022-9) and PETROBRAS-ANP-LITPEG (grant number: 0050.0078506.12.9).

**Data Availability Statement:** Data will be made available on request.

**Acknowledgments:** We gratefully acknowledge ANP/PRH-30.1 for the support. English revision by Sidney Pratt, Canadian, BA, MAT (The Johns Hopkins University), RSA dip (TEFL, Cambridge University).

**Conflicts of Interest:** The authors declare no conflict of interest.

## References

1. Lucantonio, S.; Di Giuliano, A.; Rossi, L.; Gallucci, K. Green Diesel Production via Deoxygenation Process: A Review. *Energies* **2023**, *16*, 844. [CrossRef]
2. Silva, R.J.M.C.L.; Souza, T.P.C.; Elihimas, D.R.M.; Silva, J.P.; Albuquerque, A.A.; Pacheco, J.G.A.; Silva, J.M.F. Ethanol Dehydration by Absorption and Biodiesel Production by Reactive Distillation: An Innovative Integrated Process. *Biomass Bioenergy* **2021**, *154*, 106263. [CrossRef]
3. Souza, T.P.C.; Silva, R.J.M.C.L.; Melo, J.C.; Tschoeke, I.C.P.; Silva, J.P.; Pacheco, J.G.A.; Silva, J.M.F. Kinetic Modeling of Cottonseed Oil Transesterification with Ethanol. *React. Kinet. Mech. Catal.* **2019**, *128*, 707–722. [CrossRef]
4. Eremeeva, A.M.; Kondrasheva, N.K.; Khasanov, A.F.; Oleynik, I.L. Environmentally Friendly Diesel Fuel Obtained from Vegetable Raw Materials and Hydrocarbon Crude. *Energies* **2023**, *16*, 2121. [CrossRef]
5. Kondrasheva, N.K.; Eremeeva, A. Production of Biodiesel Fuel from Vegetable Raw Materials. *J. Min. Inst.* **2023**, *260*, 248–256. [CrossRef]
6. Farias, A.F.F.; Moura, K.F.; Souza, J.K.; Lima, R.O.; Nascimento, J.D.; Cutrim, A.A.; Longo, E.; Araujo, A.S.; Carvalho-Filho, J.R.; Souza, A.G.; et al. Biodiesel obtained by ethylic transesterification using CuO, ZnO and CeO<sub>2</sub> supported on bentonite. *Fuel* **2015**, *160*, 357–365. [CrossRef]
7. de Almeida, R.P.; Aciole, R.C.G.; Infantes-Molina, A.; Rodríguez-Castellón, E.; Pacheco, J.G.A.; Barros, I.C.L. Residue-Based Activated Carbon from Passion Fruit Seed as Support to H<sub>3</sub>PW<sub>12</sub>O<sub>40</sub> for the Esterification of Oleic Acid. *J. Clean. Prod.* **2021**, *282*, 124477. [CrossRef]
8. de Oliveira, A.D.N.; Ferreira, I.M.; Jimenez, D.E.Q.; da Silva, L.S.; da Costa, A.A.F.; Pires, L.H.D.O.; Luque, R.; Osman, S.M.; Da Costa, C.E.F.; Rocha Filho, G.N.; et al. Esterification of an Agro-Industrial Waste on Kaolinite-Derived Catalyst Prepared via Microwave Irradiation. *Waste Biomass Valori.* **2022**, *13*, 3933–3944. [CrossRef]
9. Wang, Y.; Yang, Q.; Ke, L.; Peng, Y.; Liu, Y.; Wu, Q.; Tian, X.; Dai, L.; Ruan, R.; Jiang, L. Review on the Catalytic Pyrolysis of Waste Oil for the Production of Renewable Hydrocarbon Fuels. *Fuel* **2021**, *283*, 119170. [CrossRef]

10. Kurowska, K.; Marks-Bielska, R.; Bielski, S.; Kryszk, H.; Jasinskas, A. Food Security in the Context of Liquid Biofuels Production. *Energies* **2020**, *13*, 6247. [[CrossRef](#)]
11. Kumar, A.; Anushree; Kumar, J.; Bhaskar, T. Utilization of Lignin: A Sustainable and Eco-Friendly Approach. *J. Energy Inst.* **2020**, *93*, 235–271. [[CrossRef](#)]
12. Ong, H.C.; Chen, W.H.; Singh, Y.; Gan, Y.Y.; Chen, C.Y.; Show, P.L. A State-of-the-Art Review on Thermochemical Conversion of Biomass for Biofuel Production: A TG-FTIR Approach. *Energy Convers. Manag.* **2020**, *209*, 112634. [[CrossRef](#)]
13. Amaral, A.R.; Bernar, L.P.; Ferreira, C.C.; de Oliveira, R.M.; Pereira, A.M.; Pereira, L.M.; Santos, M.C.; Assunção, F.P.d.C.; Bezerra, K.C.A.; Almeida, H.S.; et al. Economic Feasibility Assessment of the Thermal Catalytic Process of Wastes: Açai Seeds (*Euterpe Oleracea*) and Scum from Grease Traps. *Energies* **2022**, *15*, 7718. [[CrossRef](#)]
14. Melo, J.A.; de Sá, M.S.; Moral, A.; Bimbela, F.; Gandía, L.M.; Wisniewski, A. Renewable Hydrocarbon Production from Waste Cottonseed Oil Pyrolysis and Catalytic Upgrading of Vapors with Mo-Co and Mo-Ni Catalysts Supported on  $\gamma$ -Al<sub>2</sub>O<sub>3</sub>. *Nanomaterials* **2021**, *11*, 1659. [[CrossRef](#)] [[PubMed](#)]
15. Azahar, A.A.; Nurhafizah, M.D.; Abdullah, N.; Ul-Hamid, A. A Review on the Palm Oil Waste Thermal Degradation Analysis and Its Kinetic Triplet Study. *Bioenergy Res.* **2023**. [[CrossRef](#)]
16. Su, G.; Mohd Zulkifli, N.W.; Ong, H.C.; Ibrahim, S.; Bu, Q.; Zhu, R. Pyrolysis of Oil Palm Wastes for Bioenergy in Malaysia: A Review. *Renew. Energ. Rev.* **2022**, *164*, 112554. [[CrossRef](#)]
17. Yu, M.; Zhang, C.; Li, X.; Liu, Y.; Li, X.; Qu, J.; Dai, J.; Zhou, C.; Yuan, Y.; Jin, Y.; et al. Pyrolysis of Vegetable Oil Soapstock in Fluidized Bed: Characteristics of Thermal Decomposition and Analysis of Pyrolysis Products. *Sci. Total Environ.* **2022**, *838*, 155412. [[CrossRef](#)] [[PubMed](#)]
18. Amaral, A.R.; Bernar, L.P.; Ferreira, C.C.; Pereira, A.M.; Dos Santos, W.G.; Pereira, L.M.; Santos, M.C.; Assunção, F.P.d.C.; Mendonça, N.M.; Pereira, J.A.R.; et al. Economic Analysis of Thermal–Catalytic Process of Palm Oil (*Elaeis Guineensis*, Jacq) and Soap Phase Residue from Neutralization Process of Palm Oil (*Elaeis Guineensis*, Jacq). *Energies* **2023**, *16*, 492. [[CrossRef](#)]
19. da Silva Almeida, H.; Correa, O.A.; Ferreira, C.C.; Ribeiro, H.J.; de Castro, D.A.R.; Pereira, M.S.; Mâncio, A.A.; Santos, M.C.; da Mota, S.A.P.; da Silva Souza, J.A.; et al. Diesel-like hydrocarbon fuels by catalytic cracking of fat, oils, and grease (FOG) from grease traps. *J. Energy Inst.* **2017**, *90*, 337–354. [[CrossRef](#)]
20. Andrade, L.A.; Barrozo, M.A.S.; Vieira, L.G.M. Thermo-chemical behavior and product formation during pyrolysis of mango seed shell. *Ind. Crops Prod.* **2016**, *85*, 174–180. [[CrossRef](#)]
21. Barbosa, J.M.; Rossi, R.A.S.; Andrade, L.A.; Barrozo, M.A.S.; Vieira, L.G.M. A study of optimization of solar pyrolysis and catalyst recovery and reuse. *Energy Conv. Managem.* **2021**, *237*, 114094. [[CrossRef](#)]
22. Bernar, L.P.; Ferreira, C.C.; Costa, A.F.; Ribeiro, H.J.; dos Santos, W.G.; Pereira, L.M.; Pereira, A.M.; Moraes, N.L.; Assunção, F.P.; Mota, S.A.; et al. Catalytic Upgrading of Residual Fat Pyrolysis Vapors over Activated Carbon Pellets into Hydrocarbons-like Fuels in a Two-Stage Reactor: Analysis of Hydrocarbons Composition and Physical-Chemistry Properties. *Energies* **2022**, *15*, 4587. [[CrossRef](#)]
23. Wisniewski, A.; Wosniak, L.; Scharf, D.R.; Wiggers, V.R.; Meier, H.F.; Simionatto, E.L. Upgrade of Biofuels Obtained from Waste Fish Oil Pyrolysis by Reactive Distillation. *J. Braz. Chem. Soc.* **2015**, *26*, 224–232. [[CrossRef](#)]
24. Kay Lup, A.N.; Abnisa, F.; Wan Daud, W.M.A.; Aroua, M.K. A Review on Reactivity and Stability of Heterogeneous Metal Catalysts for Deoxygenation of Bio-Oil Model Compounds. *J. Ind. Eng. Chem.* **2017**, *56*, 1–34. [[CrossRef](#)]
25. Su, G.; Ong, H.C.; Fattah, I.M.R.; Ok, Y.S.; Jang, J.H.; Wang, C.T. State-of-the-Art of the Pyrolysis and Co-Pyrolysis of Food Waste: Progress and Challenges. *Sci. Total Environ.* **2022**, *809*, 151170. [[CrossRef](#)]
26. Santos, T.M.; Silva, W.R.D.; Carregosa, J.D.C.; Schmitt, C.C.; Moreira, R.; Raffelt, K.; Dahmen, N.; Wisniewski, A., Jr. Thermal Conversion of Sugarcane Bagasse Coupled with Vapor Phase Hydrotreatment over Nickel-Based Catalysts: A Comprehensive Characterization of Upgraded Products. *Catalysts* **2022**, *12*, 355. [[CrossRef](#)]
27. Silva, N.K.G.; Ferreira, R.A.; Ribas, R.M.; Monteiro, R.S.; Barrozo, M.A.S.; Soares, R.R. Gas-phase hydrodeoxygenation (HDO) of guaiacol over Pt/Al<sub>2</sub>O<sub>3</sub> catalyst promoted by Nb<sub>2</sub>O<sub>5</sub>. *Fuel* **2021**, *287*, 119509. [[CrossRef](#)]
28. Hasanudin, H.; Asri, W.R.; Fanani, Z.; Adisti, S.J.; Hadiyah, F.; Maryana, R.; Al Muttaqii, M.; Zhu, Z.; Machado, N.T. Facile Fabrication of SiO<sub>2</sub>/Zr Assisted with EDTA Complexed-Impregnation and Templated Methods for Crude Palm Oil to Biofuels Conversion via Catalytic Hydrocracking. *Catalysts* **2022**, *12*, 1522. [[CrossRef](#)]
29. do Nascimento, L.A.; Barroso-Martín, L.; Peçanha, S.R.S.; Arias, S.; Santos, B.S.; Pacheco, J.G.A.; Infantes-Molina, A.; Rodríguez-Castellón, E.; Barros, I.C.L. NiAlCe Mixed Oxides Obtained from Layered Double Hydroxides Applied to Anisole Hydrodeoxygenation. *Catal. Today* **2022**, *394–396*, 282–294. [[CrossRef](#)]
30. Su, G.; Ong, H.C.; Mofijur, M.; Mahlia, T.M.I.; Ok, Y.S. Pyrolysis of Waste Oils for the Production of Biofuels: A Critical Review. *J. Hazard Mater.* **2022**, *424*, 127396. [[CrossRef](#)]
31. Dada, T.K.; Sheehan, M.; Murugavelh, S.; Antunes, E. A Review on Catalytic Pyrolysis for High-Quality Bio-Oil Production from Biomass. *Biomass Conv. Bioref.* **2023**, *13*, 2595–2614. [[CrossRef](#)]
32. da Silveira Rossi, R.A.; Barbosa, J.M.; Barrozo, M.A.S.; Vieira, L.G.M. Catalytic solar hydrolysis of the *Chlamydomonas reinhardtii* microalgae. *Biomass Bioenergy* **2021**, *152*, 106183. [[CrossRef](#)]
33. Wang, Y.; Ke, L.; Peng, Y.; Yang, Q.; Du, Z.; Dai, L.; Zhou, N.; Liu, Y.; Fu, G.; Ruan, R.; et al. Characteristics of the Catalytic Fast Pyrolysis of Vegetable Oil Soapstock for Hydrocarbon-Rich Fuel. *Energy Convers. Manag.* **2020**, *213*, 112860. [[CrossRef](#)]

34. Wang, X.; Wang, H.; Jin, X.; Wang, F.; Shen, B. Synthetic Strategies and Performance of Catalysts for Pyrolytic Production of Alternative Aviation Fuels Using Non-Edible Lipids: A Critical Review. *Appl. Catal. A Gen.* **2022**, *643*, 118769. [[CrossRef](#)]
35. Schmitt, C.C.; Fonseca, F.G.; Fraga, M.M.C.; Wisniewski, A., Jr.; Karp, S.; Mello José, A.H.; Rodrigues, R.C.L.B.; Moreira, R.; Hirayama, D.E.; Raffelt, K.; et al. Thermochemical and Catalytic Conversion Technologies for the Development of Brazilian Biomass Utilization. *Catalysts* **2021**, *11*, 1549. [[CrossRef](#)]
36. Silva, L.D.; Lira, T.S.; Xavier, T.P.; Barrozo, M.A.S.; Dantas, S.C.; Silvério, B.C.; Santos, K.G. Effect of Temperature and MgCl<sub>2</sub> Concentration on the Catalytic Pyrolysis of Malt Waste Using Response Surface Methodology. *ChemistrySelect* **2022**, *7*, e202200663. [[CrossRef](#)]
37. Silva, F.C.M.; Lima, M.S.; Costa Neto, C.O.; Sá, J.L.S.; Souza, L.D.; Caldeira, V.P.S.; Santos, A.G.D.; Luz, G.E., Jr. Catalytic deoxygenation of C18 fatty acids over HAlMCM-41 molecular sieve. *Biomass Convers. Biorefin.* **2018**, *8*, 159–167. [[CrossRef](#)]
38. Arias, S.; Vasconcelos, D.P.; Libório, D.O.; Gonzalez, J.F.; Câmara, A.G.; Barbosa, C.M.B.M.; Fréty, R.; Pacheco, J.G.A. Hydrogen-Free Deoxygenation of Industrial Vegetable Oil Waste Using Ce, Zr-NiAl Catalysts for Second-Generation Biofuels Production. *Mol. Catal.* **2022**, *529*, 112554. [[CrossRef](#)]
39. Zheng, Y.; Wang, J.; Liu, C.; Lu, Y.; Lin, X.; Li, W.; Zheng, Z. Efficient and Stable Ni-Cu Catalysts for Ex Situ Catalytic Pyrolysis Vapor Upgrading of Oleic Acid into Hydrocarbon: Effect of Catalyst Support, Process Parameters and Ni-to-Cu Mixed Ratio. *Renew. Energy* **2020**, *154*, 797–812. [[CrossRef](#)]
40. Shafizadeh, A.; Rastegari, H.; Shahbeik, H.; Mobli, H.; Pan, J.; Peng, W.; Li, G.; Tabatabaei, M.; Aghbashlo, M. A Critical Review of the Use of Nanomaterials in the Biomass Pyrolysis Process. *J. Clean. Prod.* **2023**, *400*, 136705. [[CrossRef](#)]
41. Khalid, M.A.A.; Abdullah, N.; Ibrahim, M.N.M.; Taib, R.M.; Rosid, S.J.M.; Shukri, N.M.; Yahaya, N.F.; Abdullah, W.N.B.W. Catalytic Pyrolysis of Waste Oil into Hydrocarbon Fuel Utilizing Cerium Oxide Catalyst. *Korean J. Chem. Eng.* **2022**, *39*, 1487–1495. [[CrossRef](#)]
42. Nabgan, W.; Ikram, M.; Alhassan, M.; Owgi, A.H.K.; Van Tran, T.; Parashuram, L.; Nordin, A.H.; Djellabi, R.; Jalil, A.A.; Medina, F.; et al. Bibliometric Analysis and an Overview of the Application of the Non-Precious Materials for Pyrolysis Reaction of Plastic Waste. *Arab. J. Chem.* **2023**, *16*, 104717. [[CrossRef](#)]
43. Çakman, G.; Ceylan, S.; Balci, S. Catalytic Deoxygenation of Oleic Acid over Synthesized Ni@CMK-3 Catalyst Using Analytical Py-GC/MS and TG-FTIR. *J. Porous Mater.* **2023**, *30*, 899–909. [[CrossRef](#)]
44. Arias, S.; González, J.F.; Sousa, L.V.; Barbosa, C.B.M.; Silva, A.O.S.; Fréty, R.; Pacheco, J.G.A. Influence of Ni/Al Ratio on the Fast Pyrolysis of Myristic Acid When Adsorbed on Unsupported Mixed Oxides Derived from Layered Double Hydroxides. *Catal. Today* **2021**, *381*, 181–191. [[CrossRef](#)]
45. Santos, M.R.; Sales, R.F.; Silva, A.O.S.; Teixeira, C.M.; Pacheco, J.G.A.; Fréty, R. Flash Pyrolysis of Myristic Acid Adsorbed on Supported Nickel Catalysts for Biofuel Production. *J. Therm. Anal. Calorim.* **2015**, *119*, 1875–1885. [[CrossRef](#)]
46. Hongloi, N.; Prapainainar, P.; Prapainainar, C. Review of Green Diesel Production from Fatty Acid Deoxygenation over Ni-Based Catalysts. *Mol. Catal.* **2022**, *523*, 111696. [[CrossRef](#)]
47. Zhang, Z.; Chen, H.; Wang, C.; Chen, K.; Lu, X.; Ouyang, P.; Fu, J. Efficient and Stable Cu–Ni/ZrO<sub>2</sub> Catalysts for in Situ Hydrogenation and Deoxygenation of Oleic Acid into Heptadecane Using Methanol as a Hydrogen Donor. *Fuel* **2018**, *230*, 211–217. [[CrossRef](#)]
48. Caldeira, V.P.S.; Santos, A.G.D.; Oliveira, D.S.; Lima, R.B.; Souza, L.D.; Pergher, S.B.C. Polyethylene Catalytic Cracking by Thermogravimetric Analysis: Effects of Zeolitic Properties and Homogenization Process. *J. Therm. Anal. Calorim.* **2017**, *130*, 1939–1951. [[CrossRef](#)]
49. Araújo, A.M.M.; Queiroz, G.S.M.; Maia, D.O.; Gondim, A.D.; Souza, L.D.; Fernandes, V.J.; Araujo, A.S. Fast Pyrolysis of Sunflower Oil in the Presence of Microporous and Mesoporous Materials for Production of Bio-Oil. *Catalysts* **2018**, *8*, 261. [[CrossRef](#)]
50. Qazi, U.Y.; Javid, R.; Ikhlaq, A.; Khoja, A.H.; Saleem, F. A Comprehensive Review on Zeolite Chemistry for Catalytic Conversion of Biomass/Waste into Green Fuels. *Molecules* **2022**, *27*, 8578. [[CrossRef](#)]
51. Zheng, Z.; Lei, T.; Wang, J.; Wei, Y.; Liu, X.; Yu, F.; Ji, J. Catalytic cracking of soybean oil for biofuel over  $\gamma$ -Al<sub>2</sub>O<sub>3</sub>/CaO composite catalyst. *J. Braz. Chem. Soc.* **2019**, *30*, 359–370. [[CrossRef](#)]
52. Yan, K.; Liu, Y.; Lu, Y.; Chai, J.; Sun, L. Catalytic Application of Layered Double Hydroxide-Derived Catalysts for the Conversion of Biomass-Derived Molecules. *Catal. Sci. Technol.* **2017**, *7*, 1622–1645. [[CrossRef](#)]
53. Coriolano, A.C.F.; Alves, A.A.; Araujo, R.A.; Delgado, R.C.; Carvalho, F.R.; Fernandes, V.J.; Araujo, A.S. Thermogravimetry study of the ester interchange of sunflower oil using Mg/Al layered double hydroxides (LDH) impregnated with potassium. *J. Therm. Anal. Calorim.* **2017**, *127*, 1863–1867. [[CrossRef](#)]
54. Aguilera, L.J.; Palacio, L.A.; Faro, A.C. Synthesis of NiAl Layered Double Hydroxides Intercalated with Aliphatic Dibasic Anions and Their Exchange with Heptamolybdate. *Appl. Clay Sci.* **2019**, *176*, 29–37. [[CrossRef](#)]
55. Tajuddin, N.A.; Manayil, J.C.; Lee, A.F.; Wilson, K. Alkali-free hydrothermally reconstructed NiAl layered double hydroxides for catalytic transesterification. *Catalysts* **2022**, *12*, 286. [[CrossRef](#)]
56. Cavani, F.; Trifirb, F.; Vaccari, A. Hydrotalcite-type anionic clays: Preparation, properties and applications. *Catal. Today* **1991**, *11*, 173–301. [[CrossRef](#)]
57. Lopes, D.; Zotin, F.; Palacio, L.A. Copper-Nickel Catalysts Hydrotalcite from Hydrotalcite Precursors: The Performance in NO Reduction by CO. *Appl. Catal. B* **2018**, *237*, 327–338. [[CrossRef](#)]
58. Evans, D.G.; Slade, R.C.T. Structural Aspects of Layered Double Hydroxides. *Struct. Bond.* **2005**, *119*, 1–87. [[CrossRef](#)]

59. Miyata, S. The Syntheses of Hydrotalcite-Like Compounds and their Structures and Physico-Chemical Properties I: The Systems  $Mg^{2+}-Al^{3+}-NO_3^-$ ,  $Mg^{2+}-Al^{3+}-Cl^-$ ,  $Mg^{2+}-Al^{3+}-ClO_4^-$ ,  $Ni^{2+}-Al^{3+}-Cl^-$  and  $Zn^{2+}-Al^{3+}-Cl^-$ . *Clays Clay Miner.* **1975**, *23*, 369–375. [[CrossRef](#)]
60. Kooli, F.; Chisem, I.C.; Vucelic, M.; Jones, W. Synthesis and Properties of Terephthalate and Benzoate Intercalates of Mg-Al Layered Double Hydroxides Possessing Varying Layer Charge. *Chem. Mater.* **1996**, *8*, 1969–1977. [[CrossRef](#)]
61. Rodrigues, R.M.L.; Reis, C.B.; Eon, J.G.; Palacio, L.A. Oxidative Dehydrogenation of Propane Using Ni–Mg–Al Mixed Oxide Catalysts from Hydrotalcite-Type Precursors. *Braz. J. Chem. Eng.* **2022**. [[CrossRef](#)]
62. Newman, S.P.; Jones, W. Synthesis, Characterization and Applications of Layered Double Hydroxides Containing Organic Guests. *New J. Chem.* **1998**, *22*, 105–115. [[CrossRef](#)]
63. Kim, S.C. The Catalytic Oxidation of Aromatic Hydrocarbons over Supported Metal Oxide. *J. Hazard. Mater.* **2002**, *91*, 285–299. [[CrossRef](#)] [[PubMed](#)]
64. Ashok, J.; Subrahmanyam, M.; Venugopal, A. Hydrotalcite Structure Derived Ni-Cu-Al Catalysts for the Production of  $H_2$  by  $CH_4$  Decomposition. *Int. J. Hydrog. Energy* **2008**, *33*, 2704–2713. [[CrossRef](#)]
65. Luo, L.; Yuan, F.; Zaera, F.; Zhu, Y. Catalytic Hydrogenation of Furfural to Furfuryl Alcohol on Hydrotalcite-Derived  $Cu_xNi_{3-x}AlO_y$  Mixed-Metal Oxides. *J. Catal.* **2021**, *404*, 420–429. [[CrossRef](#)]
66. Lin, X.; Zhu, H.; Huang, M.; Wan, C.; Li, D.; Jiang, L. Controlled Preparation of Ni–Cu Alloy Catalyst via Hydrotalcite-like Precursor and Its Enhanced Catalytic Performance for Methane Decomposition. *Fuel Process. Technol.* **2022**, *233*, 107271. [[CrossRef](#)]
67. Thommes, M.; Kaneko, K.; Neimark, A.V.; Olivier, J.P.; Rodriguez-Reinoso, F.; Rouquerol, J.; Sing, K.S.W. Physisorption of Gases, with Special Reference to the Evaluation of Surface Area and Pore Size Distribution (IUPAC Technical Report). *Pure Appl. Chem.* **2015**, *87*, 1051–1069. [[CrossRef](#)]
68. Khzouz, M.; Gkanas, E.I. Experimental and Numerical Study of Low Temperature Methane Steam Reforming for Hydrogen Production. *Catalysts* **2018**, *8*, 5. [[CrossRef](#)]
69. Yaakob, Z.; Bshish, A.; Ebshish, A.; Tasirin, S.M.; Alhasan, F.H. Hydrogen Production by Steam Reforming of Ethanol over Nickel Catalysts Supported on Sol Gel Made Alumina: Influence of Calcination Temperature on Supports. *Materials* **2013**, *6*, 2229–2239. [[CrossRef](#)]
70. Dragoi, B.; Ungureanu, A.; Chiriac, A.; Ciotonea, C.; Rudolf, C.; Royer, S.; Dumitriu, E. Structural and Catalytic Properties of Mono- and Bimetallic Nickel-Copper Nanoparticles Derived from  $MgNi(Cu)Al$ -LDHs under Reductive Conditions. *Appl. Catal. A Gen.* **2015**, *504*, 92–102. [[CrossRef](#)]
71. Santos, M.R.; Arias, S.; Padilha, J.F.; Carneiro, M.C.N.; Sales, E.A.; Pacheco, J.G.A.; Fréty, R. Catalytic Cracking of Palmitic and Oleic Acids Pre-Adsorbed on  $\gamma$ -Alumina. *Catal. Today* **2020**, *344*, 234–239. [[CrossRef](#)]
72. Maher, K.D.; Bressler, D.C. Pyrolysis of Triglyceride Materials for the Production of Renewable Fuels and Chemicals. *Bioresour. Technol.* **2007**, *98*, 2351–2368. [[CrossRef](#)] [[PubMed](#)]
73. Krobkrong, N.; Itthibenchapong, V.; Khongpracha, P.; Faungnawakij, K. Deoxygenation of Oleic Acid under an Inert Atmosphere Using Molybdenum Oxide-Based Catalysts. *Energy Convers. Manag.* **2018**, *167*, 1–8. [[CrossRef](#)]
74. Padilha, J.F.; Frety, R.; Santos, A.P.; Pontes, L.A.M.; Santos, M.R.; Arias, S.; Pacheco, J.G.A. Deoxygenation of Oleic Acid Methyl Ester in FCC Process Conditions Over Protonated and Sodium Exchanged Y and ZSM-5 Zeolites. *Waste Biomass Valorization* **2022**, *13*, 185–194. [[CrossRef](#)]
75. Asomaning, J.; Mussone, P.; Bressler, D.C. Pyrolysis of polyunsaturated fatty acids. *Fuel Process. Technol.* **2014**, *120*, 89–95. [[CrossRef](#)]
76. Lischka, H.; Ventura, E.; Dallos, M. The Diels-Alder Reaction of Ethene and 1,3-Butadiene: An Extended Multireference Ab Initio Investigation. *ChemPhysChem* **2004**, *5*, 1365–1371. [[CrossRef](#)] [[PubMed](#)]
77. Kubátová, A.; Št'ávoňová, J.; Seames, W.S.; Luo, Y.; Sadrameli, S.M.; Linnen, M.J.; Baglayeva, G.V.; Smoliakova, I.P.; Kozliak, E.I. Triacylglyceride Thermal Cracking: Pathways to Cyclic Hydrocarbons. *Energy Fuels* **2012**, *26*, 672–685. [[CrossRef](#)]
78. Wang, J.; Chen, Y.; Liu, C.; Lu, Y.; Lin, X.; Hou, D.; Luo, C.; Wang, D.; Zheng, Z.; Zheng, Y. Highly Stable Mo-Based Bimetallic Catalysts for Selective Deoxygenation of Oleic Acid to Fuel-like Hydrocarbons. *J. Environ. Chem. Eng.* **2023**, *11*, 109104. [[CrossRef](#)]
79. Wang, H.; Lin, H.; Zheng, Y.; Ng, S.; Brown, H.; Xia, Y. Kaolin-Based Catalyst as a Triglyceride FCC Upgrading Catalyst with High Deoxygenation, Mild Cracking, and Low Dehydrogenation Performances. *Catal. Today* **2019**, *319*, 164–171. [[CrossRef](#)]
80. Fu, L.; Li, Y.; Cui, H.; Ba, W.; Liu, Y. Highly Stable and Selective Catalytic Deoxygenation of Renewable Bio-Lipids over  $Ni/CeO_2-Al_2O_3$  for N-Alkanes. *Appl. Catal. A Gen.* **2021**, *623*, 118258. [[CrossRef](#)]
81. Billaud, F.; Minh, A.K.T.; Lozano, P.; Pioch, D. Catalytic Cracking of Octanoic Acid. *J. Anal. Appl. Pyrolysis* **2001**, *58–59*, 605–616. [[CrossRef](#)]

**Disclaimer/Publisher's Note:** The statements, opinions and data contained in all publications are solely those of the individual author(s) and contributor(s) and not of MDPI and/or the editor(s). MDPI and/or the editor(s) disclaim responsibility for any injury to people or property resulting from any ideas, methods, instructions or products referred to in the content.